Brigham Young University
BYU ScholarsArchive

Theses and Dissertations

2013-12-14

Delamination Detection in Concrete Using Disposable Impactors for Excitation

Anjali Narendra Patil
Brigham Young University - Provo

Follow this and additional works at: https://scholarsarchive.byu.edu/etd

 Part of the Electrical and Computer Engineering Commons

BYU ScholarsArchive Citation

Patil, Anjali Narendra, "Delamination Detection in Concrete Using Disposable Impactors for Excitation" (2013). *Theses and Dissertations*. 3885.
https://scholarsarchive.byu.edu/etd/3885

This Thesis is brought to you for free and open access by BYU ScholarsArchive. It has been accepted for inclusion in Theses and Dissertations by an authorized administrator of BYU ScholarsArchive. For more information, please contact scholarsarchive@byu.edu, ellen_amatangelo@byu.edu.

Delamination Detection in Concrete Using Disposable Impactors for Excitation

Anjali Patil

A thesis submitted to the faculty of
Brigham Young University
in partial fulfillment of the requirements for the degree of

Master of Science

Brian A. Mazzeo, Chair
W. Spencer Guthrie
Richard W. Christiansen

Department of Electrical and Computer Engineering

Brigham Young University

December 2013

Copyright © 2013 Anjali Patil

All Rights Reserved

ABSTRACT

Delamination Detection in Concrete Using Disposable Impactors for Excitation

Anjali Patil
Department of Electrical and Computer Engineering
Master of Science

Delaminations in concrete bridge decks result primarily from corrosion of the reinforcing bars (or rebar). This corrosion leads to volumetric expansion of the rebar. When the rebar expands, concrete cracks, and there is a localized separation of the concrete cover from the underlying concrete. Impact-echo testing is an effective technique to map delaminations on concrete bridge decks. However, mapping speed is limited by necessary retrieval of the impactor for traditional tests. To achieve higher scanning speeds, it is advantageous to use both a non-contact measurement (air-coupled impact-echo) and disposable-impactor excitation. Disposable impactors have the potential advantage of achieving greater deck scanning speeds because they do not need to be retrieved, and they can also be used with air-coupled measurement systems.

This thesis reports impact excitation of concrete using disposable impactors such as water droplets and ice balls. The impact characteristics of these impactors are compared with those of steel balls and chain links. Comparing the acoustic recordings on intact and delaminated concrete surface shows that water droplets and ice balls are able to excite flexural resonant modes associated with delamination defects. The use of water droplets and ice balls for shallow delamination detection in concrete is thus demonstrated.

Keywords: concrete, corrosion, delamination, bridge deck, air-coupled, impact-echo, disposable impactors, flexural mode

ACKNOWLEDGMENTS

Foremost, I wish to express my gratitude to my advisor Dr. Brian Mazzeo at Brigham Young University for all the guidance and inspiration during my graduate study. He not only acted as thesis advisor and a committee chair, but also as a mentor who has spent many long hours helping in my development as a student and person. Without his guidance and valuable insight, this thesis would not have been completed. I would also like to thank Dr. Guthrie (Department of Civil and Environmental Engineering) for providing valuable advice, materials, and tools for the research. I really appreciate the assistance and technology from Randy Hurd (research assistant in Department of Mechanical Engineering) and Dr. Truscott (Department of Mechanical Engineering) for the high-speed photography. I would like to extend my thanks to the Department of Electrical and Computer Enginnering and the Department of Civil and Environmental Engineering for their support throughout this research.

Staff members, my friends, and my fellow graduate students in the Department of Electrical and Computer Engineering also deserve special thanks. I am immensely grateful to my husband, Dr. Nikhil Churi, for his incredible encouragement and support throughout my graduate studies. Last, but not least, I would like to thank my parents for their love and continuous support through my life.

Table of Contents

List of Tables

List of Figures

Chapter 1

Introduction

Corrosion and aging of bridge decks around the world are pressing issues that will require large interventions by responsible governments to ensure the safety and reliability of these structures [1]. Inspection of bridge decks is an important component of bridge management, as rehabilitation and replacement resources must be allocated according to the severity of the problem and the risk to public safety. While new automated methods are being developed, bridge deck inspection can be time-consuming and subjective and often requires multiple instruments and measurement techniques to produce conclusions about the relative health of the bridge [2, 3]. This thesis demonstrates an air-coupled impact-echo technique aimed to reduce the time and subjectivity associated with mapping delamination defects on bridges.

1.1 Significance of Bridge Deck Inspection

An alarming number of bridges in the United States are structurally deficient and currently require billions of dollars for repair and rehabilitation [4]. To program restoration activities in a rational approach and in a reduced-budget environment, risk-based maintenance, rehabilitation, and replacement (MR&R) strategies are being implemented to prioritize projects by national and state agencies [5]. Successful implementation of these strategies requires programming the right kinds of MR&R treatements at the right time [6]; thus, cost-effective, timely, and accurate assessments of bridges are needed.

Of all bridge elements, the deck is the most susceptible to deterioration. Because of its direct exposure to vehicular traffic and natural weathering, it continuously deteriorates in service and requires regular maintenance [7]. In regions where winter deck maintenance involves routine applications of chloride-based deicers, reinforcing steel in concrete bridge decks

is more likely to experience corrosion due to chloride penetration down to the rebar mat [8]. As corrosion occurs, the steel expands in volume due to oxidation [9]. The volume expansion causes tensile forces around the rebar, and, because concrete has low tensile strength (Figure 1.1), cracking of the surrounding concrete takes place [9]. The corrosion-induced cracking process is illustrated in Figure 1.2. Cracking that results in a subsurface separation of the upper portion of the concrete from the lower portion of the concrete, often at the level of the top rebar mat, causes internal voids called delaminations [10]. As the damage becomes more extensive, cracking becomes visible on the surface, the concrete spalls, and eventually a pothole forms. These surface conditions further accelerate corrosion because the concrete no longer protects the rebar from chloride ingress, and significant corrective actions must be implemented to preserve the deck [11]. The ability to accurately determine the type and scope of work appropriate for preserving a deck depends on the ability to accurately assess its condition, as proper timing of certain treatments, such as overlay applications, are critical for the successful management of bridges [12].

(a) Concrete under compressive force

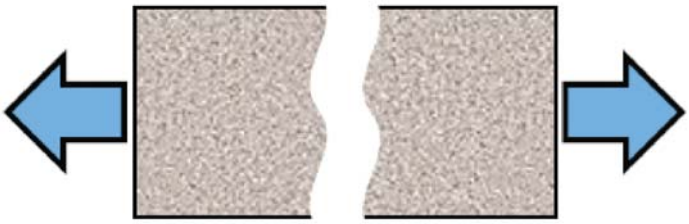

(b) Concrete under tensile force

Figure 1.1: (a) Concrete has excellent compressive strength. (b) Concrete has low tensile strength and breaks easily under tensile forces.

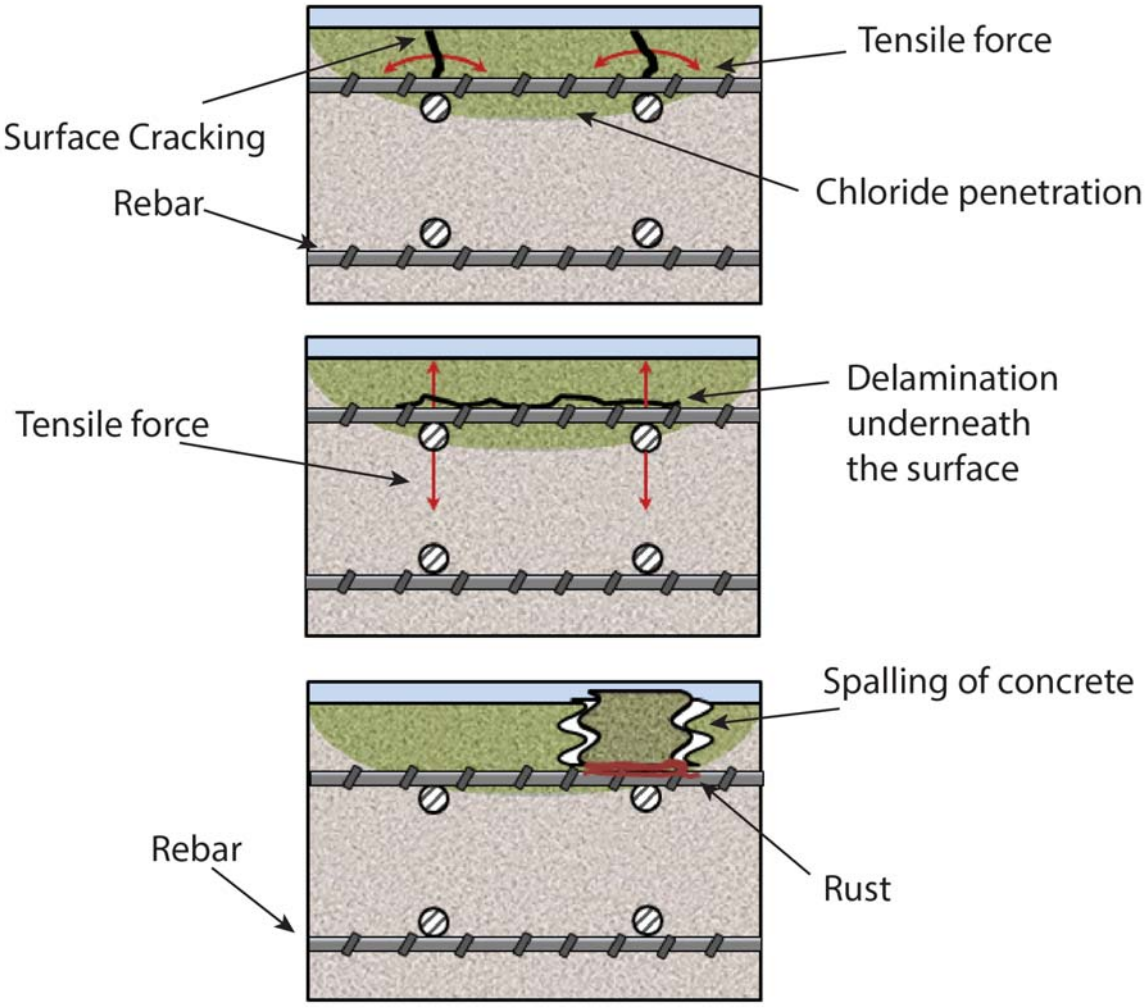

Figure 1.2: Corrosion-induced cracking process in concrete.

Unfortunately, much of the deterioration on a bridge deck cannot be visually inspected because it is below the surface [13]. While it is now recognized that multiple evaluation methods must be combined to better characterize concrete bridge decks [14], chain dragging and hammer sounding are still the mainstays of most bridge deck inspection programs because operators can "hear" the voids in the deck [15]. However, these techniques are both subjective and resource-intensive, as they typically involve multiple technicians, necessitate manual transcription of data, and frequently require traffic control and lane closures [13].

1.2 Research Problem

To characterize the structural integrity of bridge decks, many nondestructive techniques such as ground-penetrating radar, acoustics, ultrasonic methods, electrochemical methods, and spectrographic imaging methods are used [13]. Of these, acoustic-based impact-echo has proven to be a highly effective method for identifying internal defects in concrete. Originally developed at the National Institute of Standards and Technology in the 1980s [16], the impact-echo technique is traditionally employed by striking the surface and listening to the response using piezoelectric surface sensors [17]. The major difficulty with this form of impact-echo testing is that it is a point measurement, and coupling the sensors to the concrete surface greatly limits deck scanning speeds. Recently, impact-echo surface wave and acoustic sounding have been combined in a single scanning unit. However, so far the maximum reported speeds achieved are only 2.4 km/h [18], and a traditional excitation approch is employed. More recently, air-coupled impact-echo testing has received attention because the absence of surface sensors can potentially increase the speed of data collection [19, 20, 21, 22, 23, 24, 25, 26]. Use of parabolic reflectors further enhances the air-coupled technique by gathering more of the emitted acoustic signal [27]. However, non-contact excitation of the acoustic modes in concrete is difficult because of the high acoustic impedance mismatch between air and concrete [28]; therefore, almost all experiments are performed by using steel ball impactors for excitation of concrete. Wheeled devices that perform this type of excitation are demonstrated in the literature [13, 29].

In all of these cases, however, the necessary retrieval of the impactor after its contact with the concrete surface greatly limits the speed of deck testing. Therefore, it appears necessary to search for alternative excitation techniques that can be combined with non-contact measurement methods to improve deck scanning speeds. While there have been many developments reported on the use of advanced signal processing methods to increase the accuracy of flaw detection, such as noise cancellation techniques [28, 30], less attention has been given to methods of excitation. The excitation techniques are limited to the use of sounding hammers, steel balls, or solenoids. To increase the deck scanning speed and to avoid the necessary retrieval of the impactors, use of disposable impactors in combination with non-contact measurement is demonstrated in this thesis.

1.3 Thesis Statement

To overcome the problem of subsequent retrieval of the impactor, this thesis proposes the use of disposable impactors, such as water droplets and ice balls, to excite the acoustic responses necessary for detection of shallow delaminations in concrete. The impact characteristics of different sizes of disposable impactors are studied and compared with those of standard steel balls. It is demonstrated that an acoustic excitation using water droplets and ice balls in combination with non-contact measurement has great potential for use in automated bridge deck inspection.

1.4 Thesis Outline

The outline of this thesis is as follows. Chapter 2 provides background information. This includes the theory of the impact-echo method and Hertzian low-velocity impact theory for the solid-solid impacts. It further covers relevant literature about the acoustic responses of impacts. Chapter 3 describes the use of water droplets for excitation of acoustic responses. Chapter 4 describes the use of ice balls as disposable impactors to detect delaminations. In Chapter 5, impact characteristics of ice balls on intact and delaminated concrete are compared with those of standard steel balls and chain links. It also contains mapping of a sample deck slab using steel balls and ice balls for shallow delamination detection. Finally, the conclusion and future research directions are provided in Chapter 6.

Chapter 2

Theory of Impact-echo Testing

2.1 A Brief History of Impact-echo Testing

Visual inspection and sounding methods such as chain dragging are the most widely used nondestructive test (NDT) methods for evaluating the structural health of concrete. Visual inspection is limited in that only those defects within the view of operator can be located. Involving a degree of subjectivity, chain dragging is described by ASTM standard D4580 for detecting delaminations in concrete bridge decks [15]. An experienced operator is required to detect meaningful changes in the acoustic reponse of the deck, and thus its accuracy can be affected by operator fatigue. Chain dragging often requires traffic control and lane closures [13].

Quantitative impact-echo testing is another NDT method that has proven to be a highly effective method for identifying internal defects in concrete. The testing was developed in the 1980s at the National Institute of Standards and Technology [16] and is traditionally employed by applying a transient point load on the concrete surface using a metal ball or hammer and then listening to the acoustic response. This method facilitates interrogation of a variety of defects within the concrete, particularly when a peizoelectric transducer is mounted on the surface [17]. Zhu and Popovics demonstrated the use of an air-coupled transducer, which permit measurements of "leaky" surface waves in the concrete that emit acoustic energy into air; thus, measurements could be performed without any surface contact [19]. Zhu et al. showed that use of parabolic reflectors further enhances the air-coupled technique by gathering more of the emitted acoustic signal [27]. The use of parabolic reflectors improves the signal-to-noise ratio in air-coupled impact-echo measurements [27]. Because different NDT techniques must be used in conjunction with each other,

more recently, air-coupled impact-echo testing has been jointly demonstrated with infrared thermography [22].

2.2 Overview of Impact-echo

In the impact-echo technique, P-waves, or compression waves, are induced at the testing surface using a short-duration mechanical impact. The propagating P-waves and their reflections (from boundaries or internal defects) result in surface displacement. A schematic of impact-echo testing is presented in Figure 2.1. The surface displacement is recorded using a surface-mounted transducer, and the data are often analyzed in the frequency domain.

2.3 Ideal Solid-Solid Hertzian Impacts

As the theory of solid-solid impacts has been treated extensively in the scientific literature [31, 32], a basic model of solid-solid impacts is available for describing the force-time characteristics of an impact event. For all of our experiments with air-coupled impact-echo testing, gravity is used for acceleration of the impactors over relatively short distances, as opposed to the use of compressed gas for particle acceleration, for example [33]. This limits the impactor velocities to < 7 m/s. Under these conditions, Hertzian contact theory can be applied to such low-velocity, solid-solid impacts.

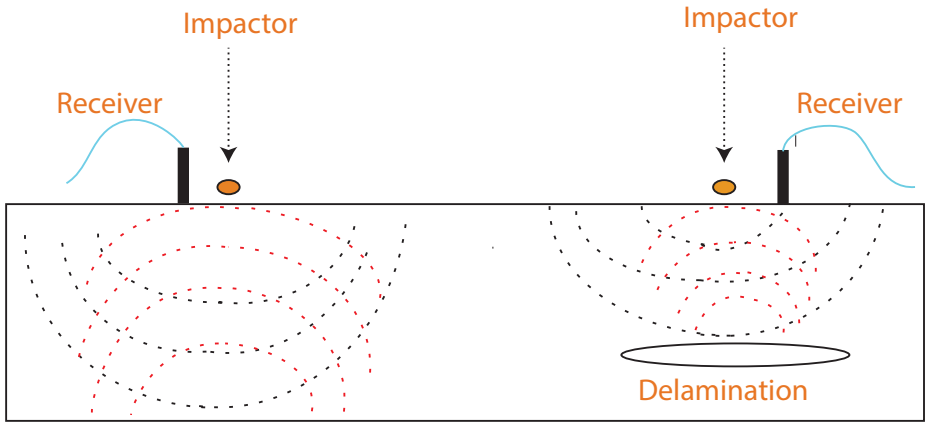

Figure 2.1: Impact-echo relies on acoustic waves being reflected by acoustic discontinuities corresponding to delaminations or voids in the material.

The developement in [32] is followed here for the impact of a spherical ball on an infinite plate. Using the material parameters of the spherical ball and plate, the effective modulus of the combined system, E_*, is defined as

$$E_* = [(1-\nu_B^2)E_B^{-1} + (1-\nu_{B'}^2)E_{B'}^{-1}]^{-1}, \tag{2.1}$$

where E_B and ν_B are the elastic modulus and Poisson's ratio of the impacting ball and $E_{B'}$ and $\nu_{B'}$ are the elastic modulus and Poisson's ratio of the plate. The combined stiffness, κ_S, is then given as

$$\kappa_S = \frac{4}{3}\, E_* \sqrt{R_*}, \tag{2.2}$$

where R_* is the effective radius of the ball and plate, which in the case of a ball and infinite plate is just the radius of the ball. The total kinetic energy of the impact, T_0, is given as

$$T_0 = \frac{1}{2}\, m_B V_0^2, \tag{2.3}$$

where m_B is the mass of the ball and V_0 is the velocity of the ball at the time of impact. Integration of the equations of relative motion and application of spherical contact theory are required to solve for the force and time relations [32]. Using these values, we can then calculate the largest contact force exerted on the plate, F_c, from the expression

$$F_c = 1.73\, \kappa_S^{2/5} T_0^{3/5}. \tag{2.4}$$

The contact radius, a_C, can then be determined from the effective stiffness and maximum force by

$$a_C = \left[\frac{F_c}{\kappa_S}\right]^{1/3} \sqrt{R_*}, \tag{2.5}$$

and the maximum indentation, δ_C, is given as

$$\delta_C = a_C^2 / R_*. \tag{2.6}$$

The contact time until maximum deformation, t_C can then be estimated through numerical integration [32] as

$$t_C = 1.47\,\delta_C/V_0. \tag{2.7}$$

If the collision is perfectly elastic, then the total contact time will be $2t_C$. The maximum force can then be expressed in terms of the ball material properties, velocity, radius and the plate material properties as

$$F_c = 3.025[(1-\nu_B)^2 E_B^{-1} + (1-\nu_{B'})^2 E_{B'}^{-1}]^{-2/5} R_*^2 \sigma_B^{3/5} V_0^{6/5}, \tag{2.8}$$

where σ_B is the density of the ball. Equation 2.8 shows that, if the ball material and the plate material have very different elastic moduli, the mechanical properties of the material with the smaller elastic modulus will dominate the maximum force. Therefore, in the case of steel-concrete impacts, where steel has an elastic modulus of 200 GPa and concrete has an elastic modulus of 30 GPa, the concrete properties will more strongly influence the peak force for a given impact. In the case of ice-concrete impacts, although the difference in elastic moduli between the two materials is comparatively smaller, the properties of the ice will dominate the peak force. For an impactor with a given radius, the equation also demonstrates that a denser object, such as steel (7850 kg/m^3), will also produce a much stronger peak force than a less dense object, such as ice (920 kg/m^3). Increasing the velocity of the impactor is advantageous in all cases for increasing the force. The contact time can also be found from algebraically manipulating and rearranging Equation 2.8 as shown by Mclaskey and Glaser in [34]

$$t_C = 2.538[(1-\nu_B)^2 E_B^{-1} + (1-\nu_{B'})^2 E_{B'}^{-1}]^{2/5} R_* \sigma_B^{2/5} V_0^{-1/5}. \tag{2.9}$$

This expression shows that reducing the effective elastic modulus of the combined system, reducing the impact velocity, or increasing the size or the density of the ball will increase the contact time [35]. The contact time is an important consideration for the type of impact pulse applied to the concrete because it specifies the range of frequencies that will be excited. The development followed here additionally considers that the force-time curve of the linearly

approximated Hertzian impact can be characterized as

$$F(t) = F_C \sin\left(\frac{\pi t}{2\,t_C}\right), \tag{2.10}$$

where t is time [32]. This is a linear approximation that would change the constant of 1.73 in Equation 2.4 with full integral form to a constant of 1.48 [32]. There is still active academic inquiry in the area of contact mechanics and the nature of the force-time impact relationship. In the impact-echo literature, many different excitations are used in numerical simulations. For example, Tsai and Zhu used $\sin^2(\pi t/t_C)$ [24], Oh [36] and Zhang and Xie used $\sin^3(\pi t/t_C)$ [37], McLaskey and Glaser used $\sin^{3/2}(\pi t/t_C)$ [34], while others such as Liu and Yeh have used the half-sine expressed in Equation 2.10 [38]. The diversity of force-time relations in the literature reflects the complicated nature of impacts and the evolving understanding of solid-solid impacts as they relate to impact-echo simulations. In simulations, most researchers simulate perpendicular point loading at the impact location; however, distributed loading effects and lateral displacements and forces must also occur due to the nature of the curved contact surface [39]. However, despite these complications, the Hertzian relationships presented above serve as guidance to estimate the applied forces and residence times during an actual impact.

2.4 Reflections at Boundaries or Internal Defects

On concrete bridge decks specifically, once the ball has actually impacted the concrete, various transfers of energy occur. Most of the energy is not returned as part of the acoustic reponse but is dissipated into the concrete [40]. In addition, some energy is absorbed through deformation of the ball, which, in the case of an ice ball, may even crack. During impact, the concrete is indented, and various waves emanate from the impact point. The fastest travelling pressure waves (P-waves) associated with a normal stress reflect off of boundaries or internal defects [16]. The amplitude of reflection depends on the specific acoustic impedance of interface materials and is quantified by a reflection coefficient. The reflection coefficient, R_N, for normal incidence is given by the formula [41]:

$$R_N = \frac{z_2 - z_1}{z_2 + z_1}, \tag{2.11}$$

where z_1 and z_2 are the specific acoustic impedances of material 1 and material 2 at the interface, respectively. The approximate values of specific acoustic impedances for some materials are listed in Table 2.1. Putting the values of specific acoustic impedances from Table 2.1 in Equation 2.11, reflection coefficients for the interface of concrete with respect to the material are obtained, and the values are listed in column 1 of Table 2.1. The large difference in specific acoustic impedance for a concrete-air interface result in an absolute reflection coefficient of 1, which causes total reflection of an incident P-wave at the interface. It is this property of a concrete-air interface that enables detection of delaminations or voids in concrete [17]. For the concrete-steel interface, less than total reflection is observed. This means that the reflections from a concrete-air interface (defects or external boundaries) will be different than the reflections from a concrete-steel interface [42].

2.5 Vibration Modes of a Plate

Generally, the high-frequency waves associated with P-waves being reflected off the bottom of a plate specimen or embedded defects [16] are actually zero-group-velocity Lamb waves that radiate acoustic energy into the air [43, 44]. In addition to the Lamb waves, low-frequency flexural modes representing the plate vibrations of the concrete are excited.

Table 2.1: Reflection coefficients and acoustic impedances of different materials for compression waves travelling through concrete

Material	Reflection Coefficient	Specific Acoustic Impedance (kg/m^{2}s)
Air	-1.00	412
Concrete	0	7-10 $\times 10^6$
Steel	0.65 to 0.75	47×10^6
Water	-0.65 to -0.75	1.48×10^6
Soil	-0.30 to -0.90	0.3-4 $\times 10^6$

While some recent simulations predict the first symmetric zero-group-velocity Lamb wave mode to have a larger amplitude than flexural modes, the lower frequency flexural modes actually had much larger energy content in the associated experiments [24]. In simulations of ideal delaminations, the energy of the vibrational modes has been shown to be considerably smaller than that of the flexural modes when the side-to-depth ratio of defects is > 5 [36]. For practical purposes, given that only fairly large delaminations (generally greater than 300 mm in diameter) will actually be detected and repaired on a bridge deck, the flexural mode response associated with larger area and side-to-depth ratio defects may be of greater importance in rapid, large-area scanning operations for initial bridge deck characterization studies.

2.5.1 Frequency Response for Plate Thickness Mode

For impact-echo testing, the thickness mode frequency is given by the formula:

$$f = \beta \frac{C_P}{nd}, \tag{2.12}$$

where f is the fundamental thickness mode frequency, β is the "Lamb wave" correction factor, C_P is the P-wave velocity, d is the distance to the reflecting interface and n is a constant factor of 2 for air-filled delaminations [40]. The value of the correction factor β is often taken to be 0.96 according to Sansalone and the ASTM standard [16, 45] and verified by Zhu and Popovics [46]. Therefore, the above formula can be used to calculate the depth d of the reflecting interface if the thickness mode frequency f is known from frequency domain analysis of the data taken over delamination. However, the plate thickness mode analysis cannot be applied to the flexural modes.

2.5.2 Frequency Response for Flexural Mode

Closed-form solutions for the dynamic response of delaminated or void structures are not available [36]. This is because classical vibration theory depends on the type of geometry, plate thickness, boundary conditions, etc., which in turn affect the flexural vibration analysis [36]. Therefore, the frequency response of shallow or near-surface delaminations can

be approximated by assuming the geometry, aerial size, and boundary conditions. It has been demonstrated that the flexural vibrations fall between a simply supported boundary condition and a clamped boundary condition [36]. Assuming a thin plate circular geometry for shallow delaminations, we can estimate the natural frequencies by using the following formulas [47]:

$$\omega_{\text{clamped}} = \frac{11.84}{a^2}\sqrt{\frac{h^2 E_{B'}}{12\rho(1-\nu_{B'}^2)}}, f_{\text{clamped}} = \frac{\omega_{\text{clamped}}}{2\pi}, \tag{2.13}$$

$$\omega_{\text{supported}} = \frac{5.90}{a^2}\sqrt{\frac{h^2 E_{B'}}{12\rho(1-\nu_{B'}^2)}}, f_{\text{supported}} = \frac{\omega_{\text{supported}}}{2\pi}, \tag{2.14}$$

where a is the diameter of the plate, h is the plate thickness, f_{clamped} is the fundamental frequency for the clamped case, and $f_{\text{supported}}$ is the fundamental frequency for the simply supported case.

The frequency estimations are only approximate and depend on the aerial size, shape, and depth of the delamination defect. These frequency estimations will be used to interpret results in subsequent chapters.

Chapter 3

Delamination Detection in Concrete Using Liquid Droplets for Excitation

Perhaps the most easily deployed, least expensive, environmentally safe, and plentiful means of acoustic excitation are water droplets. Although the acoustics of rain drops falling into liquid pools has been studied for well over a hundred years [48], the acoustic response of drops falling onto solids is less well understood. In traditional impact-echo testing, excitation of the acoustic waves in the concrete is generally performed by a special hammer or a steel ball bearing [49]. Liquid drops can also produce the impact necessary for acoustic excitation [50]. For the rigid solid surface, the impact pressure P generated in a liquid-solid impact is given by [51]:

$$P = \rho C V, \tag{3.1}$$

where C and ρ are the acoustic velocity and the density of the undisturbed liquid, respectively, and V is the impact velocity. This is an approximation based on one-dimensional "water hammer" theory. While solutions for the liquid-drop impact problem have existed for many years [51, 52], recent numerical models show how the impact force evolves over the time of the impact event [53]. A much larger pressure can be generated than expected for a simple water column because of the high acoustic velocity in water (approximately 1497 m/s for fresh water [54]). It is also obvious from the literature that the liquid-solid impact is a complicated event that is an active area of research in theoretical and numerical studies [55]. The important point is that a pressure wave can be produced in the concrete by the liquid drop impact that can interrogate the concrete similar to a ball bearing using the impact-echo method as described in Chapter 2.

We have used droplets instead of a continuous flow because the stagnation pressure of a continuous jet is much less than the initial water hammer pressure during impact [56, 57].

Producing droplets that are uniform in size is also a challenge [58, 59]. An optimal faucet that balances the viscosity and surface properties to produce large liquid drops is thus necessary for a desired high flow rate [60]. Just as different ball bearing sizes produce different acoustic responses, different droplet sizes will have different excitation profiles because of their different peak pressures at a given location [51, 61]. Low velocity fluid flow is necessary to avoid jetting and to produce droplets that are sufficiently large to produce sufficient impacts [58].

To increase the velocity of the droplets, gravity can be used to accelerate the drops. Increasing the velocity substantially increases the impact pressure and thus the magnitude of the resulting acoustic response of the material. A pressure wave emanating from the surface of the concrete can then be detected by traditional microphones.

Acoustic excitation using falling water droplets is demonstrated to excite the resonant modes associated with shallow or near-surface delaminations in concrete. Slow and fast water flows produce large and small droplets with varying impact parameters. Spectrograms of acquired acoustic data demonstrate the effectiveness of the technique to detect concrete delaminations. Photography reveals the size differences of the droplets.

3.1 Apparatus and Experiment

A schematic of the apparatus that was created to provide the simultaneous excitation and measurement of the acoustic signals is presented in Figure 3.2. Water to be used is stored in a tank on the cart. An Iwaki RD-05H pump is used to pump the water up through flexible tubing, having an inner diameter of 6 mm, to the discharge head at the top of the pole. A flow meter (Mason Flow Controls FM-1142) is used to regulate the flow rate of water. The distance from the floor to the water orifice is 2.0 m.

In this experimentation, a delamination in the laboratory floor in FB-110 (on-grade concrete) that had previously been mapped by a chain-drag survey was tested together with nearby intact concrete not containing any delaminations. The delaminated laboratory floor is shown in Figure 3.1. The delamination occurred at the location of a previous concrete surface repair, the thickness of which was estimated to be less than 2 cm; destructive examination of the laboratory floor was not performed. The impact areas for the falling drops were

Figure 3.1: Photograph of the delaminated on-grade concrete floor in laboratory FB-110 (Harvey Fletcher Building, Brigham Young University campus).

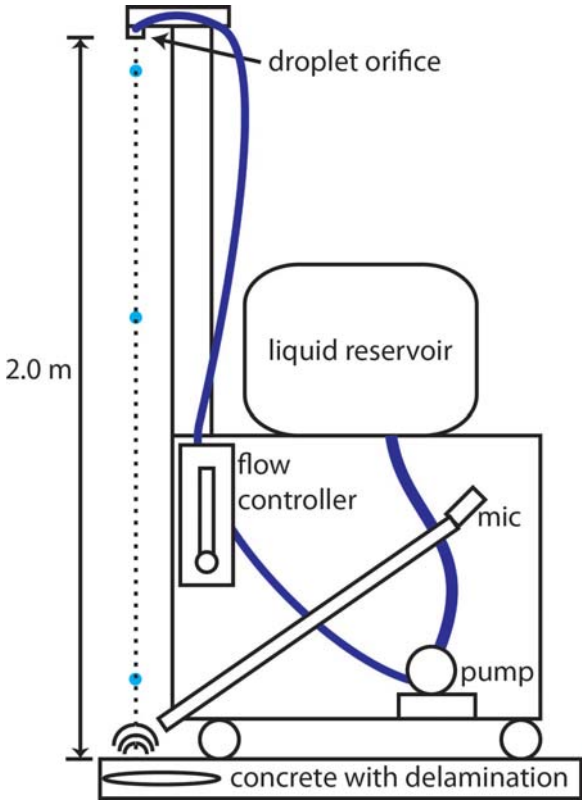

Figure 3.2: Cart schematic used for acoustic excitation and measurement of the impact-echo response of water droplets on concrete surface

approximately 25 cm^2. The orifice was positioned over the intact and delaminated concrete locations, and responses were recorded at different flow rates.

For these experiments the flow of droplets was begun, and then the acoustic data were recorded continuously for a few seconds without any specific triggering caused by the droplet release or impact. To preserve all the recorded spectral data for subsequent processing, recordings were stored as wave files without compression.

A single continuous recording was post-processed in MATLAB to produce a spectrogram of the acquired signal by using a sliding 2048-point Hamming window to compute a 2048-point Fourier transform of each window. The number of points was selected based on efficient 2^n-point Fast Fourier Transform algorithms to accurately capture both low- and high-frequency responses. An overlap of 1900 points was also used to enhance temporal resolution of the acoustic signals so that impacts and responses could be observed clearly and compared without subsequent time registration of the impacts. The power spectral density was estimated, and the resulting continuous spectrogram for one recording was plotted.

Photographs of the falling water droplets were taken with a Nikon D40 with exposure times of 1/400 or 1/500 second with $f/5.6$ and a focal length of $55.0\,mm$ using an $18-55$ mm lens and camera flash. To ensure that splashes did not hit the lens of the camera, exposures were taken from a distance of about 1.5 m from the impact point.

3.2 Results and Discussion

Two flow rates are demonstrated here that produce different drop sizes and different acoustic responses. The slow flow rate was regulated at 22.5 mL/min, and the high flow rate was regulated at 94 mL/min. Photographs illustrating the two different flow rates are given in Figure 3.3, which shows that the water drops falling at the fast flow rate are much smaller than those falling at the slow flow rate.

The spectrograms associated with the slow fluid flow rate are found in Figure 3.4 and clearly show how individual droplet impacts are recorded with great clarity. In this data, it is apparent that a flexural resonant mode of the delamination is found at about 1.5 kHz. Also a noticable echo with a peak at the same resonant frequency appears to be associated with the splash of the drop. Low-frequency noise below 1 kHz is also visible and is consistent

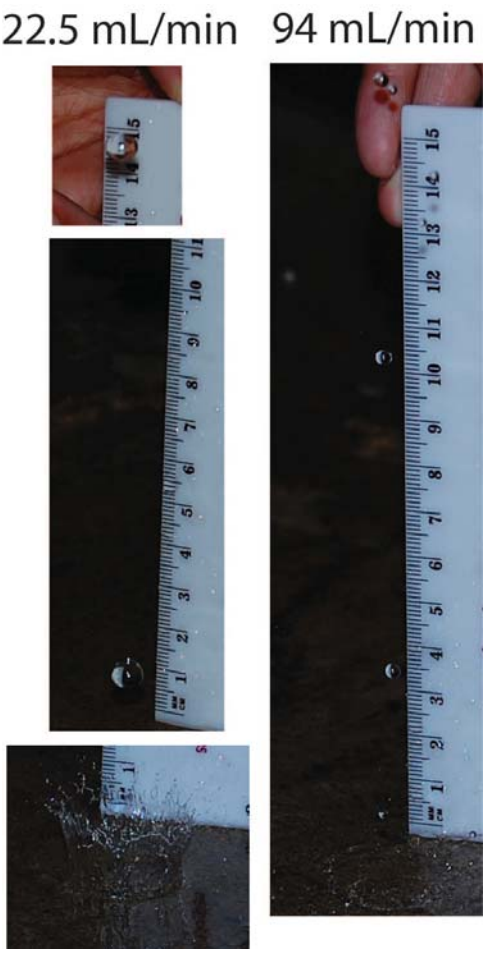

Figure 3.3: Photographs of water droplets falling at two different flow rates. The droplets on the left have diameters of approximately $7-8$ mm, while the drops on the right have diameters of approximately 3 mm.

with the ambient noise found in the laboratory environment, as well as the fluid pump. From these data the drops are calculated to arrive at a rate of approximately $2.3-2.4$ drops/s. This corresponds to approximately 0.163 cm^3/drop, approximately the same volume as a 7-mm-diameter spherical drop (0.180 cm^3).

The spectrograms associated with the fast fluid flow are found in Figure 3.5 and also clearly show how the acoustic response changes when droplets strike a delamination. In this case, the acoustic response is less attributable to individual impacts, but more to the continual impacts of multiple drops. The response of an individual drop is thus much less pronounced. This is due to the decreased kinetic energy associated with each drop and also the reduced peak pressure that may be attributed to increased droplet curvature [51].

However, there are many more drops compared to the slow fluid flow configuration, so the total signal associated with the delamination is still strong.

There are advantages and disadvantages to slow and fast droplet flow rates. When the droplet flow rate is slow, the individual impacts can be resolved without overlap. For the fixed orifice, a slow flow rate also means larger drops, which have a greater impact force per drop that greatly aids the researcher trying to understand the response of an individual drop. It is also more comparable to traditional impact-echo tests with a single impulse. The background noise is also quite visible when the slow rates are used and can be visually or computationally removed.

Fast flow rates produce an almost "white noise" excitation of the acoustic modes and blend the individual impact responses, especially for the flexural mode exhibited in this experimentation, into a continual tone, which may be more easily observed as the cart moves. This is likely the regime that would be implemented in the field to quickly produce many impacts over large areas during a scan. However, collisions between falling drops and splashes from previous impacts do seem to be more prevalent and produce a larger variance in the impact responses, as displayed in the spectrograms. Because of these interactions, individual droplet responses cannot necessarily be used to represent all of the observed phenomena in the fast, multiple-droplet, flow regime.

The acoustic frequency response of individual impacts extends up to the experimental Nyquist frequency of 25.6 kHz, so there may be possibilities for excitation of higher-frequency resonant modes other than the dominant flexural mode that is characteristic of this shallow delamination [17]. Size of the droplet and speed of impact, just as size and drop height of ball bearings in traditional impact-echo testing, will also influence the frequency response. Further tests on controlled concrete substrates as well as numerical modeling of the impacts will be needed to establish the usable frequency range and depth of penetration of this technique. Additionally, the details of acoustic impact responses by droplets arriving at non-perpendicular angles and/or affected by wind together with surface roughness and hydrophobicity are areas of research that need to be explored. These considerations will be important for deployment of the technique on concrete structures in the field.

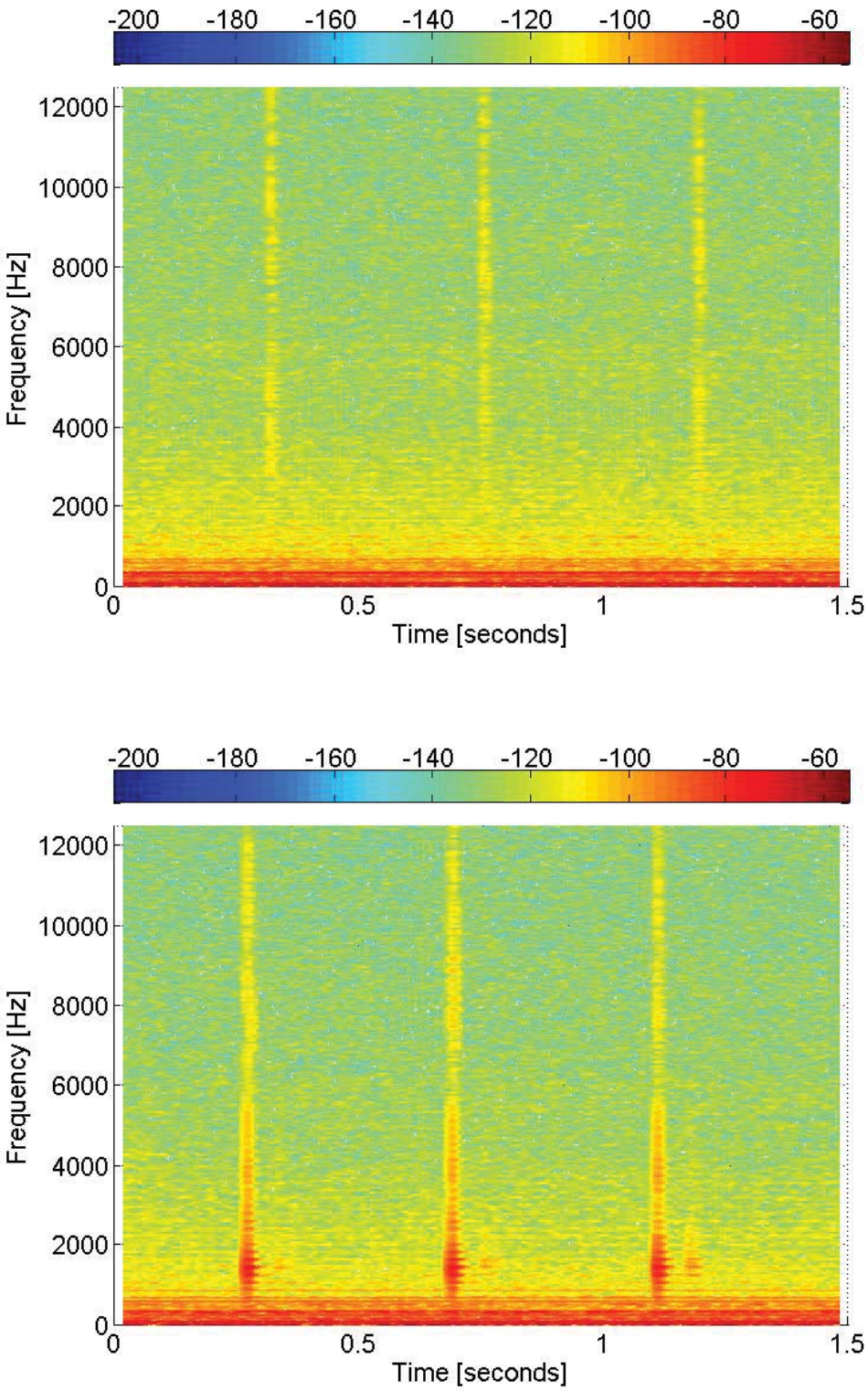

Figure 3.4: Spectrograms of acoustic data recorded at the slow (22.5 mL/min) flow rate. The top spectrogram was recorded over intact concrete, while the bottom spectrogram was recorded over a delamination. The color bar indicates the sound level in dB. The low-frequency acoustic modes associated with the delamination are readily apparent in the spectrograms.

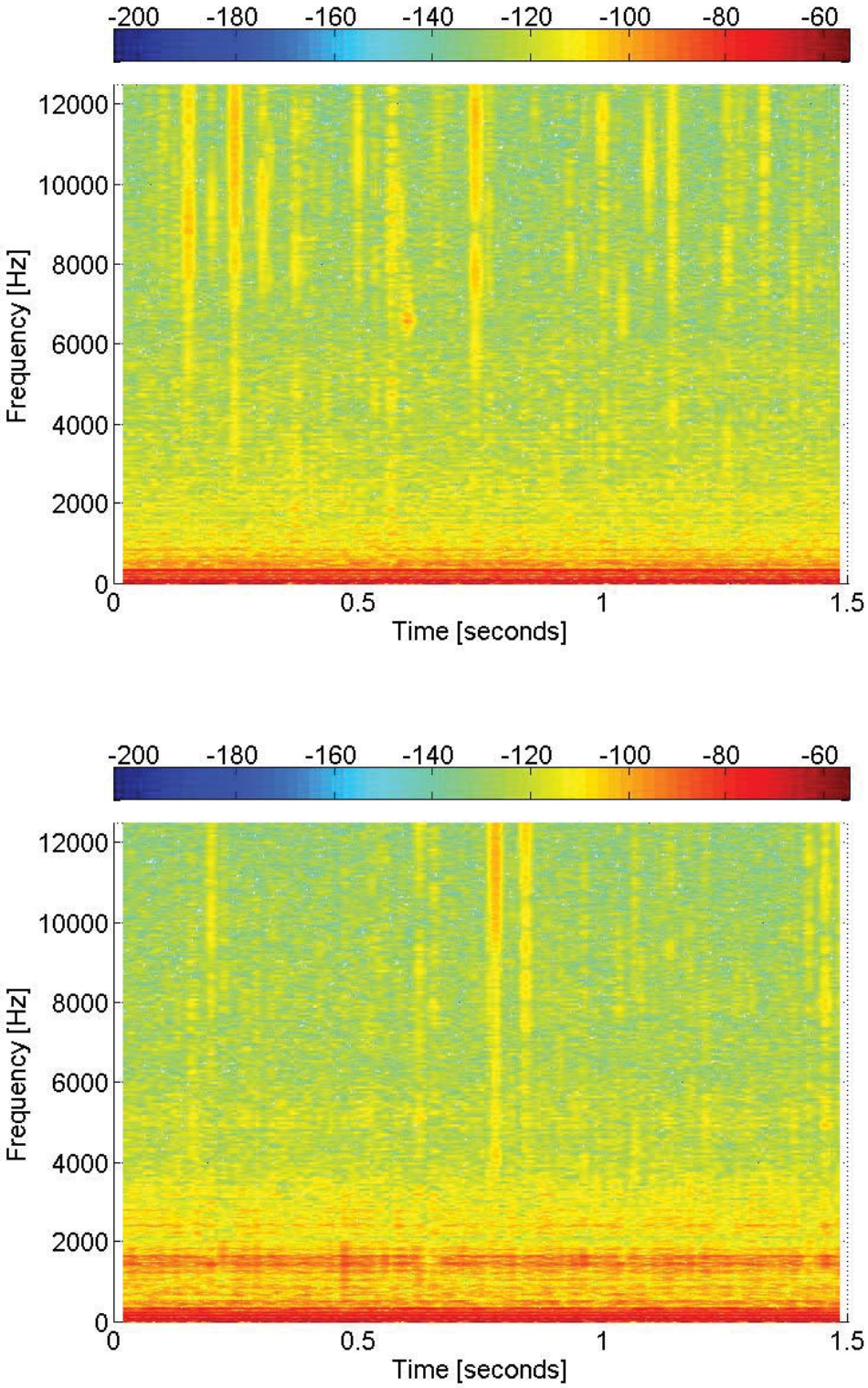

Figure 3.5: Spectrograms of acoustic data recorded at the high (94 mL/min) flow rate. The top spectrogram was recorded over intact concrete, while the bottom spectrogram was recorded over a delamination. The color bar indicates the sound level in dB. The low-frequency acoustic modes associated with the delamination are readily apparent in the spectrograms.

3.3 Conclusion

The data clearly show that the droplets can excite the acoustic modes in the concrete associated with delaminations. Thus, this technique is recommended as a non-retrieval method of excitation. Liquids are attractive impactors because water is easily spread over the surface. Solid de-icers such as sodium chloride, calcium chloride, and calcium magnesium acetate pellets have also been used in impact-echo tests to produce impacts. Like the liquid droplets, they also produce clear acoustic responses. Although bulk material handling may be more difficult in the field when solid de-icers are used, they have advantages for use in weather conditions where freezing water may be problematic. Also, the impact force of low-velocity droplets is orders of magnitude below that of a solid-solid impact [62], which would restrict the use of low-velocity droplets in the field.

To improve this technique, formation of optimized droplets will have to be studied, particularly with respect to modifying density, viscosity, and surface tension properties to enhance the interrogation of concrete. Additionally, optimizing the location of the microphone and collection of the acoustic signal will be important for the deployment in the field. Signal processing techniques will also be employed to classify impacts [63] and to reduce the noise [30] that will be present in the signals.

The use of droplets for acoustic excitation of materials is thus demonstrated to be a promising non-destructive interrogation technique that can be used in situations where mechanical coupling to the material is undesirable.

Chapter 4

Delamination Detection in Concrete Using Spheres of Ice for Excitation

While the use of water in liquid form may be insufficient for detecting deep delaminations typical of those on bridge decks, its use in solid form has great potential. Ice spheres made from potable water are disposable as well as environmentally friendly. When applied during warm seasons, ice would melt away quickly following deck testing and would therefore have minimal adverse effects on the safety of the traveling public. Given these potential benefits, the objective of this set of experiments was to investigate the use of ice spheres as impactors for delamination detection in concrete by comparing their impact characteristics with those of standard steel balls.

The mechanical properties of ice have been studied extensively in the scientific literature [64, 65]. While the properties of ice are derived from its crystalline microstructure, ice in nature and in artificial preparations is generally polycrystalline in form unless the ice is specially grown [66]. Polycrystalline ice has a bulk modulus of 8.9 GPa, a Young's modulus of 9.3 GPa, a shear modulus of 3.5 GPa, and a Poisson's ratio of 0.33 [67]. For spheres dropped on a hard substrate such as thick glass, the critical velocity for ice fragmentation is very low (between 1.5 and 3 m/s for ball diameters between 10 and 45 mm) [68]; the probability of fragmentation increases with increasing speed and ball size [69].

Natural hail has been the subject of numerous studies on this topic [70]. Hailstones often have diameters greater than 1 cm with terminal velocities higher than 10 m/s [71]. As hail gets larger, its terminal velocity increases, and speeds greater than 20 m/s can be observed [72]. Severe thunderstorms are classified by the National Weather Service as those storms having hailstone diameters greater than 2.54 cm [73]. Above this threshold, damage to roofing materials on buildings is highly probable [74]. Involving even higher speeds,

hail collisions with aircraft have also been studied experimentally for many years [75], with great concern for potential damage to engines, instruments, or the aircraft body [76]. At speeds over 50 m/s, hailstone impacts can cause significant damage, especially to composite materials [77, 78].

These studies demonstrate the potential importance of the size and velocity characteristics of ice impactors for impact-echo testing of concrete bridge decks. For active sensing schemes, ice parameters could be selected and engineered specifically for a particular sensing modality. As an example, transportation application protocols have already been developed for the delivery, storage, and dispensing of ice as needed for controlling the temperature of concrete at the time of concrete batching [79, 80].

Simultaneous acoustic recordings and high-speed photography of representative low-velocity impacts with parametric analysis have been used to compare impact characteristics of steel balls and ice spheres on intact and delaminated concrete. These results agree qualitatively with Hertzian contact theory for low-velocity impacts. Excitation of concrete using continuous impacts of ice spheres of multiple sizes and a feature extraction procedure based on time-frequency analysis allows the acoustic signature of delaminations to be classified. The use of ice as an impactor for stochastic excitation of acoustic modes in concrete is thus demonstrated.

4.1 Material and Experimental Method

Experiments were performed on a $2.75\,\mathrm{m} \times 1.5\,\mathrm{m} \times 0.215\,\mathrm{m}$ deck slab shown in Figure 4.1. It was removed from the deck of a decommissioned bridge in Provo, Utah, just prior to its demolition in 2012 as part of the Interstate 15 reconstruction project. The bridge was constructed in 1937 using uncoated reinforcing steel. Because of the many delaminations that formed during its 75 years of service, the sample deck slab was an ideal test subject for this research. Further, it complements previous research by others who have also used recovered bridge decks [13]. Figure 4.2 shows the side view of two areas along one edge of the slab that were selected for testing. A chain drag was used to confirm that the uncracked section was intact and that the cracked section was delaminated at the target test locations on the slab surface.

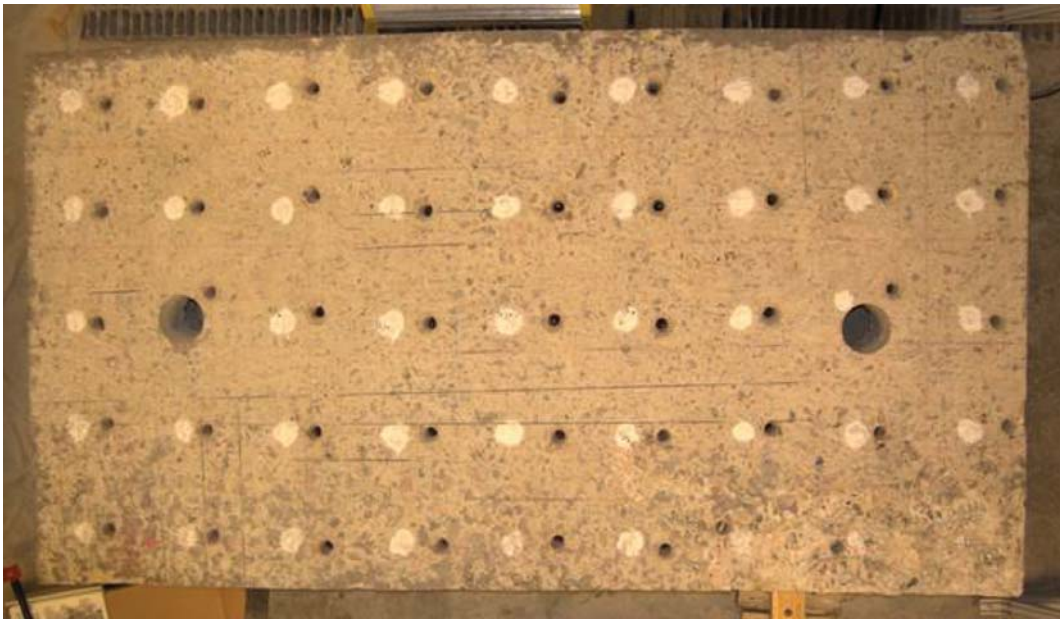

Figure 4.1: Photograph of the 2.75 m × 1.5 m × 0.215 m slab of concrete obtained from decommissioned bridge deck on Interstate 15 in Provo, Utah.

Figure 4.2: Intact and delaminated test locations on the concrete bridge deck sample.

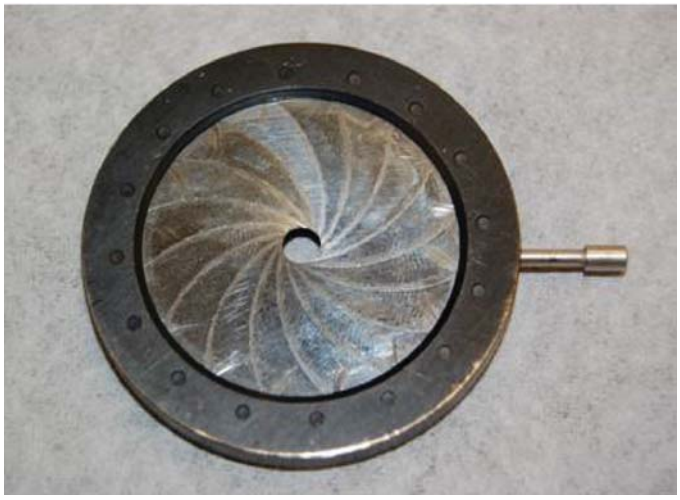

Figure 4.3: Photograph of a circular diaphragm aperture used to release ball bearings and ice balls consistently.

To release the ball bearings and ice spheres consistently, a circular diaphragm aperture as shown in Figure 4.3 was mounted 10 cm above the slab surface. The schematic of the setup is as shown in Figure 4.4. A microphone was also mounted above the concrete to record the acoustic response. A high-speed camera was positioned on the side of the bridge deck slab so that the center of the camera aperture was parallel to the concrete surface, and a small mirror was used to redirect a high-intensity LED spotlight into the camera lens (Figure 4.5). A steel ball bearing, having a mass of 18.8 gm and a radius of 8.3 mm, was used as a reference impactor, and ice spheres each having a mass of 10.413 $\pm$ 0.043 g (n=6) and a radius of 14 mm were fabricated by freezing tap water in a 24-ball tray mold (Hutzler) in a standard freezer.

A piezotronics 130E20 array microphone (6-mm diameter, free-field, bandwidth from 20 Hz to 20 kHz ($\pm$5 dB), $>$ 122 dB dynamic range, Transducer Electronic Data Sheet (TEDs) compliant) was mounted about 12 cm away from the impact point and directed towards the impact location. The signals were recorded with an acoustic sampling unit (National Instruments 9234) in a compactRIO system (National Instruments) connected to a computer. A LabVIEW virtual instrument controlled the data acquisition on the computer. The acoustic data were then postprocessed in MATLAB to produce spectrograms of impacts.

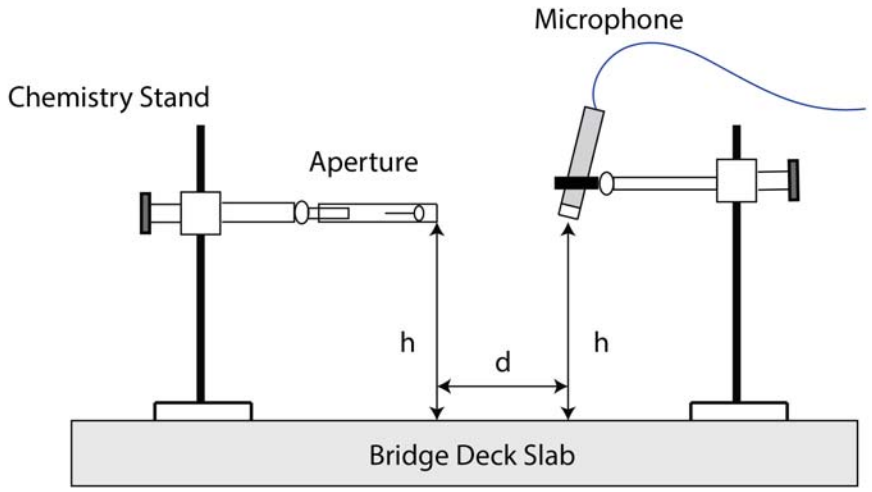

Figure 4.4: Two chemistry stands used to position the aperture and microphone on the bridge deck slab (lateral displacement d~5 cm and drop height h~10 cm).

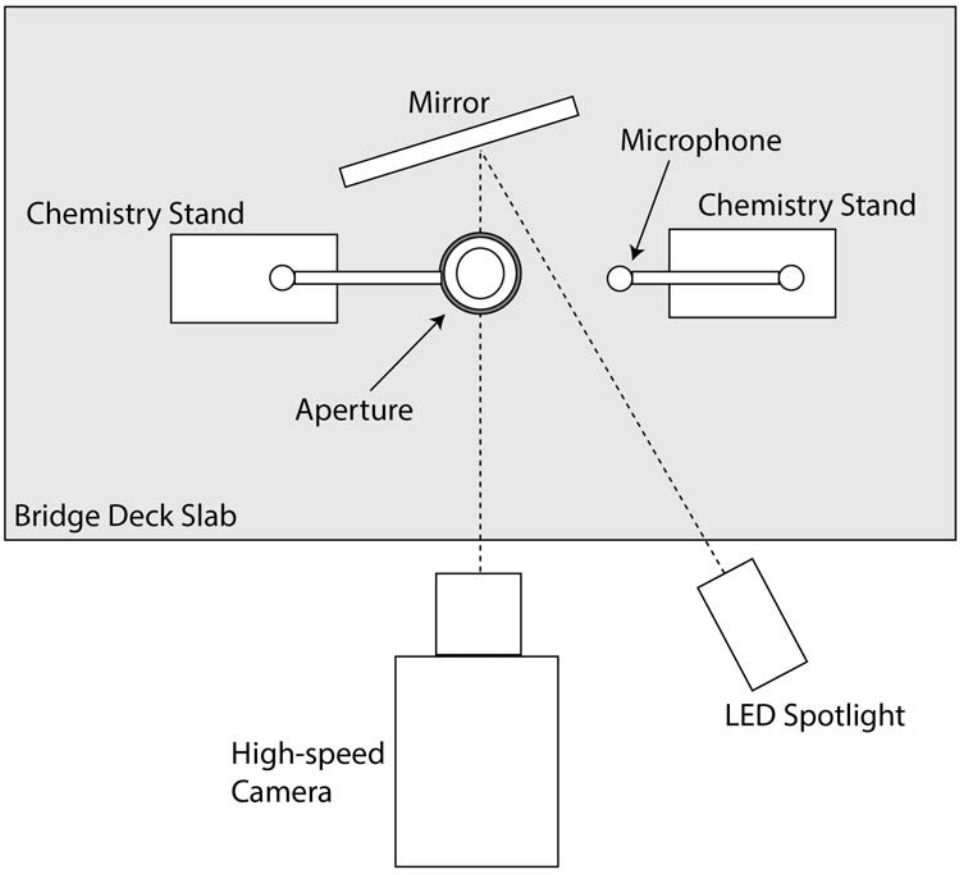

Figure 4.5: High-speed camera positioned on the side of the bridge deck slab and the small mirror used to redirect a high intensity LED spotlight into the camera lens.

A sliding 512-point Hamming window with 450 overlap points was used to compute the 512-point periodogram of the acoustic data, and the power spectral density was estimated.

To visually record the impacts, a Photron APX high-speed photographic system was used with a 50-mm Nikon lens focused on the impact area. Images were captured at a rate of 250 kfps and analyzed using MATLAB. A Sobel edge detection algorithm with parametric fitting was employed to locate the edge of the ball bearing or ice sphere in each frame. Linear fitting of the velocities was performed for 600 μs directly preceding the start of the residence time on the surface as well as for 600 μs directly following the end of the residence time. This time interval was chosen to produce linear fits before the effects of gravity greatly influenced the linearity of the curves, making them quadratic; the start and stop times were manually determined and are only approximate. From these velocities, the energy dissipated by the impact was computed from the difference in kinetic energies before and after impact. The kinematic coefficient of restitution was calculated by dividing the rebound speed by the impact speed. The average force associated with each impact was computed from the mass and acceleration of the impactor, the latter being estimated by dividing the change in velocity by the residence time.

As a further demonstration of the technique, multiple ice spheres ranging in radius from 14 to 20 mm were released from a height of 1.7 m above intact and delaminated areas of concrete, and the acoustic response was recorded as in the previous experiments.

4.2 Results

From the high-speed video, a sequence of selected images 200 μs apart is shown in Figure 4.6 with the associated parametric fits to the ball in the image. The calculated trajectories of the impactors are plotted in Figure 4.7. The acoustic spectrograms for the initial impacts of steel ball bearings on intact and delaminated surfaces are shown in Figure 4.8 (a) and Figure 4.8 (b), respectively, while corresponding acoustic spectrograms for the initial impacts of ice spheres are shown in Figure 4.8 (c) and Figure 4.8 (d). Subsequent bounces were not analyzed. The raw acoustic data for the ice sphere impacts on intact and delaminated areas are shown in Figure 4.9 (a) and Figure 4.9 (b).

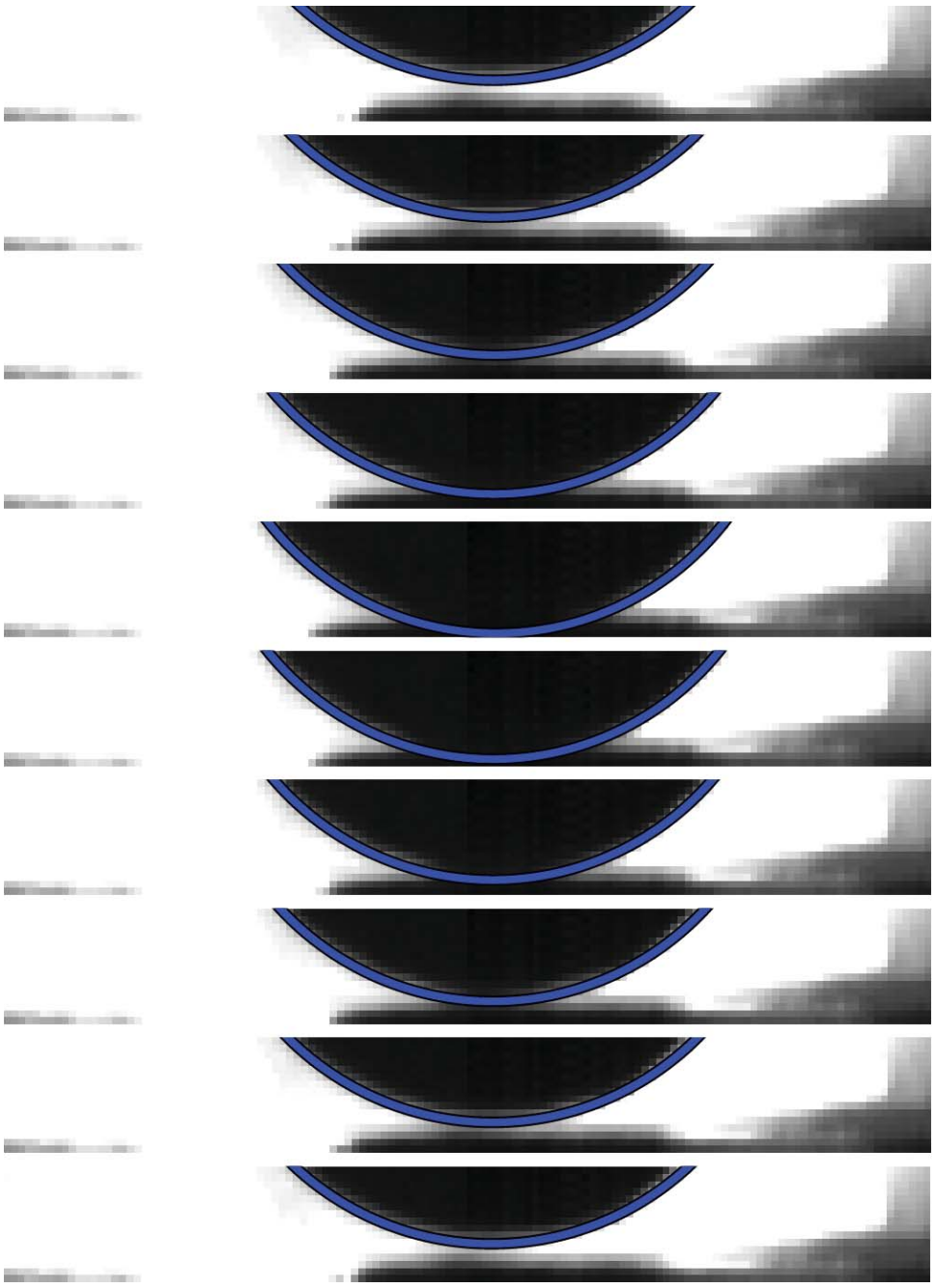

Figure 4.6: Images of ball bearing impact on delaminated concrete from high-speed video at 250 kfps. The estimated position of the ball bearing after image processing is outlined with the blue circle. The images are 200 μs apart.

For the tests with multiple ice spheres of varying diameters, the computed spectrograms associated with these impacts over a period of 1 s are presented in Figure 4.10 (a) and

Figure 4.10 (b). In these plots the frequency scale was reduced to emphasize the primary low-frequency resonance (at 1.4 kHz) clearly associated with the delamination.

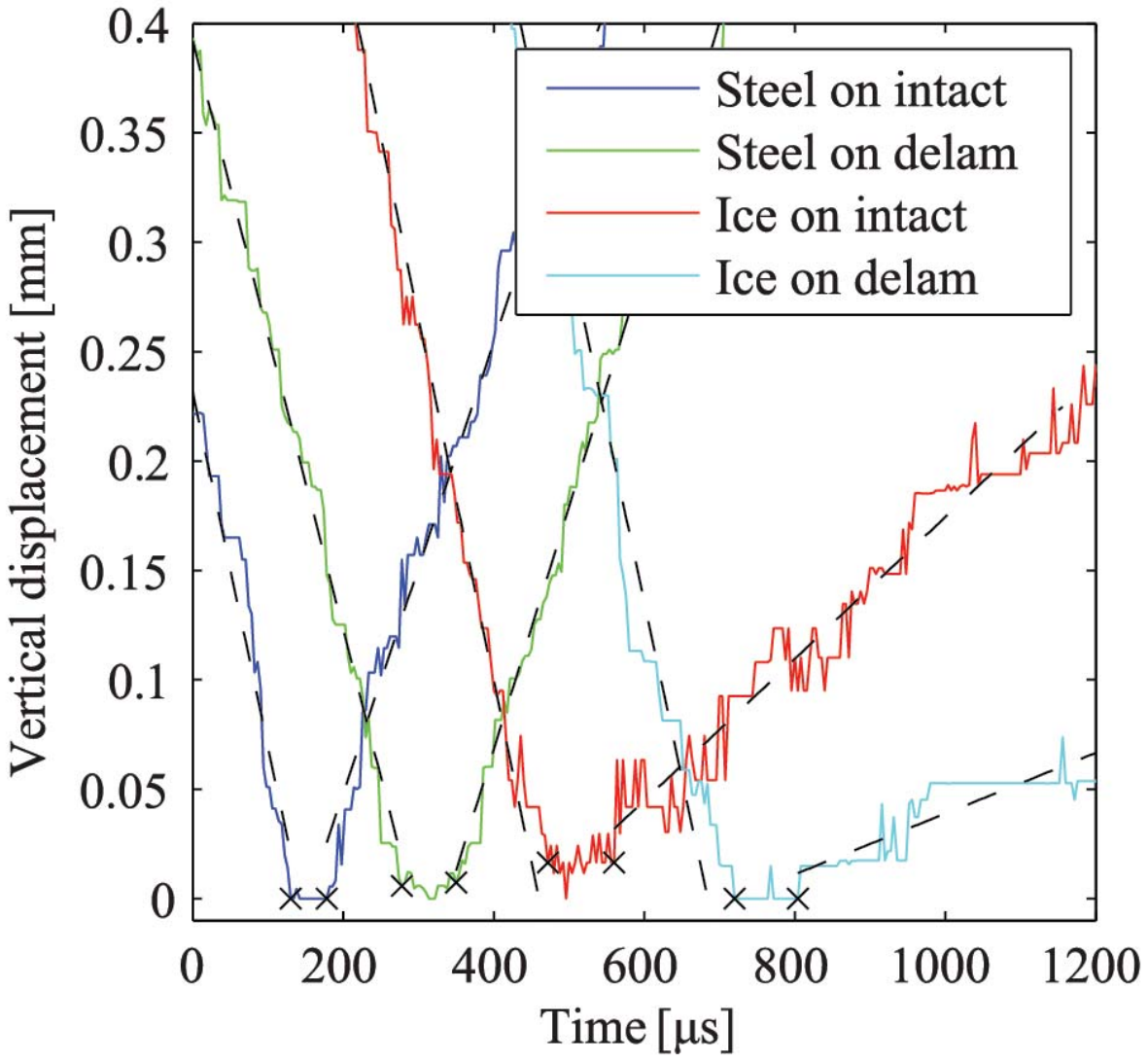

Figure 4.7: Trajectories of ball bearings and ice spheres recorded from videos. The velocities of the impactors were estimated (dashed lines) from 600 μs before and after the residence times, the beginning and ending of which are each marked by an "x" in the plot .

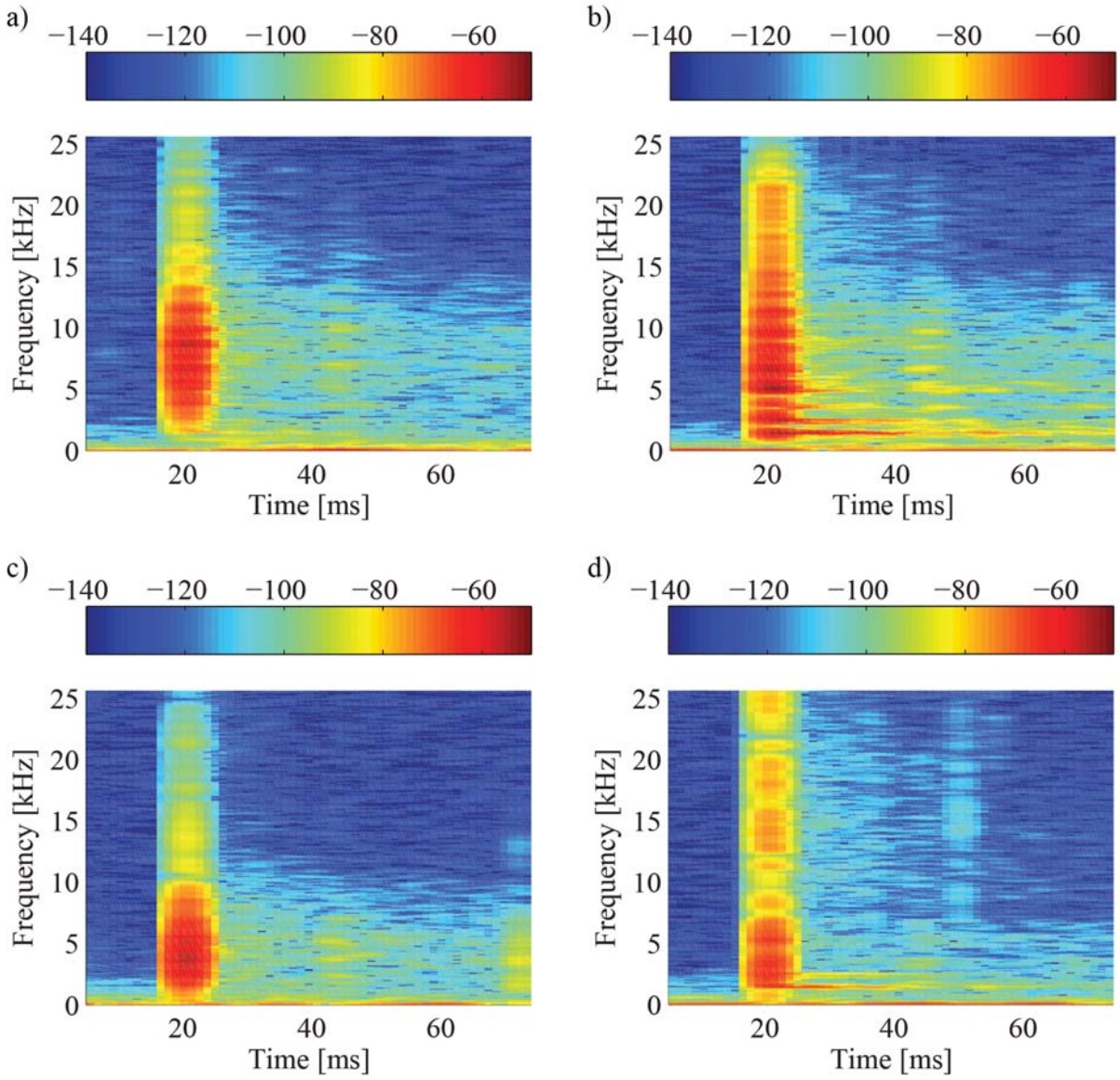

Figure 4.8: Spectrogram of ball bearing impacts on (a) intact and (b) delaminated areas of concrete. The low-frequency responses continue well after the original impact sound has ocurred in the delaminated case. Spectrograms of ice sphere impacts on (c) intact and (d) delaminated areas of concrete. The ice spheres also excite the low-frequency modes that were observed with the ball bearing impacts on the delaminated area. The scale is in dB.

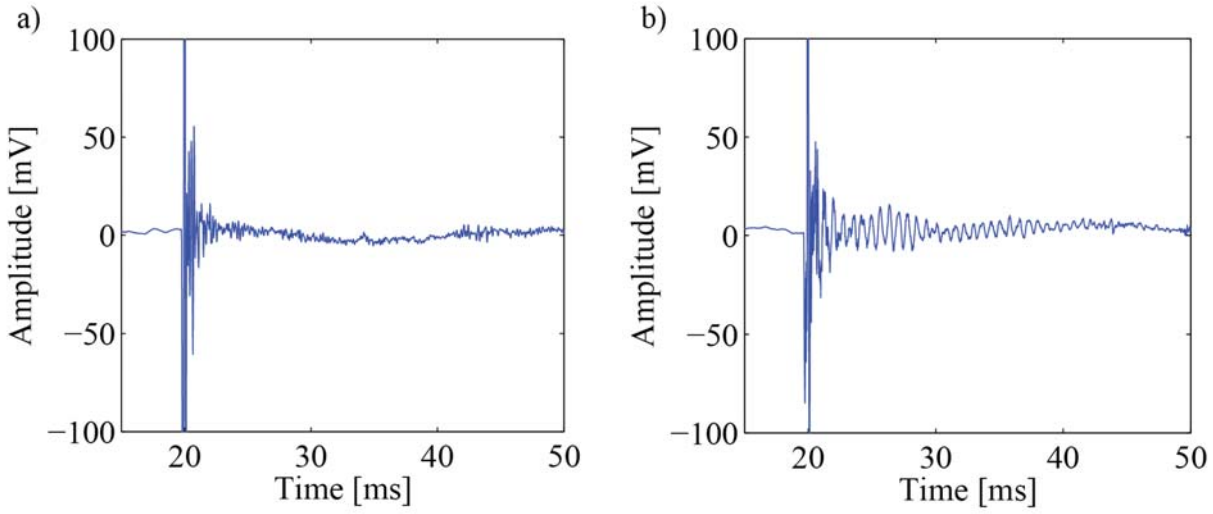

Figure 4.9: Raw acoustic data from the impacts of ice spheres on (a) intact and (b) delaminated areas of concrete taken over the same time period as in Figure 4.8. It is evident that the low-frequency response is excited and decays visibly in the delaminated case.

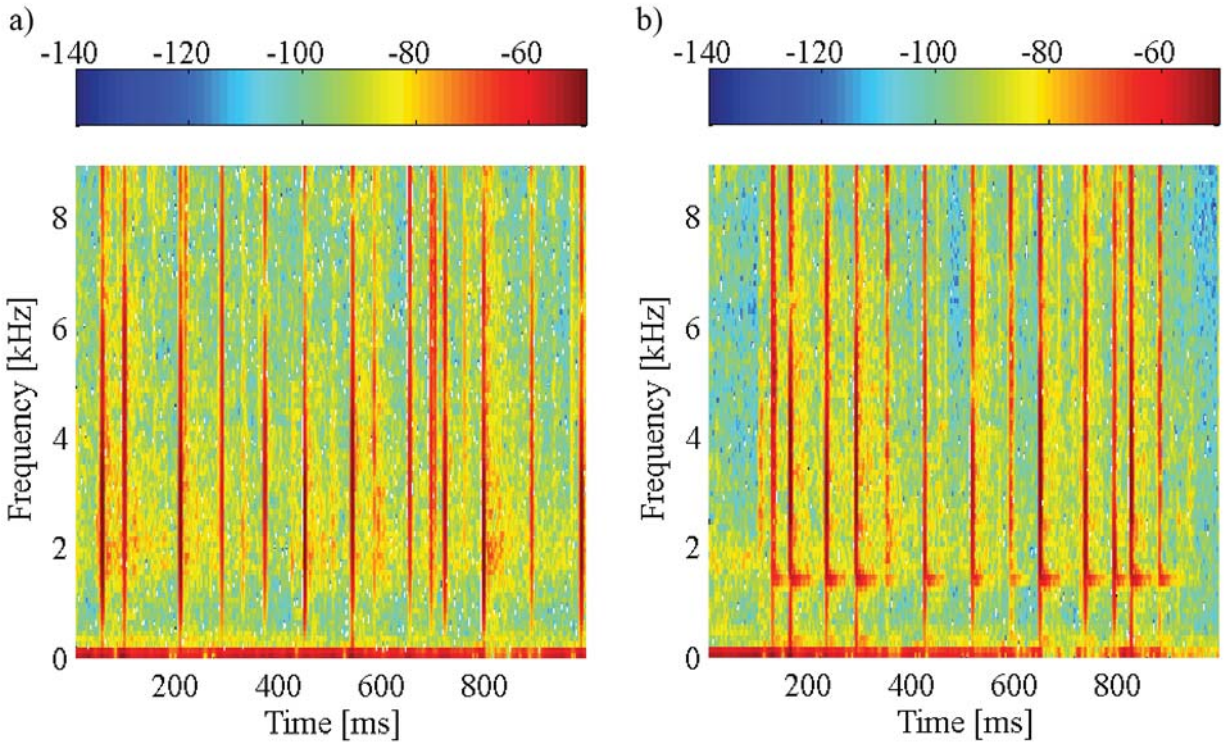

Figure 4.10: Spectrograms of multiple ice sphere impacts on (a) intact and (b) delaminated areas of concrete. Low-frequency responses are easily observed in the delaminated case. The scale is in dB.

4.3 Discussion

The discussion is divided into two parts concerning the analysis of the single impacts at low height and velocity and the continuous impacts of multiple ice spheres at greater hight and velocity.

4.3.1 Single Steel and Ice Impacts on Concrete

In Figure 4.11, power spectral densities are computed for acoustic responses of a ball bearing and ice sphere on an intact portion of the slab. For the impacts near the center of the slab, the measured peak frequency for the ball bearing impact response is 9.84 kHz. It is clear that the steel ball bearing excites a higher set of frequencies than the ice sphere, the impact of which seems to concentrate energy at lower frequency of about 4.9 kHz. This is the reason that the impact-echo fundamental mode is much less prominent in the spectrum produced by the ice ball impact.

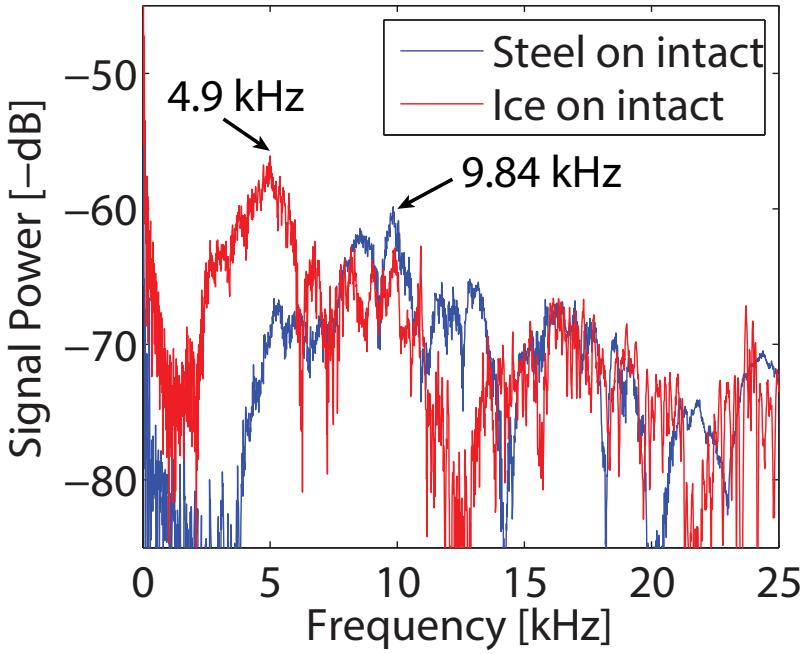

Figure 4.11: Power spectral density of an impact of a ball bearing (blue) and the impact of an ice sphere (red) on an intact surface of the concrete slab near the center of the slab. The frequency with maximum energy for the ball bearing impact is 9.84 kHz.

The results of the calculations, given in Table 4.1, show that the residence times for the ice spheres were approximately 15 to 85 percent greater than those for the ball bearings, with the greatest difference occurring over intact concrete. Because of the cracking of ice spheres after impact, the magnitude of energy dissipated through their impacts ranged from about 5 percent less to 150 percent more than that dissipated through impacts of the ball bearings, with the largest difference occurring over delaminated concrete is this case. Finally, the results also indicate that, in this experiment, the ice spheres generated an average force approximately 65 to 80 percent less than that of the ball bearings, attributable in part to the lower mass of the ice spheres; heavier ice spheres could be used to generate more force, as needed.

It is noted that the estimated density of the ice used was slightly less than that of ideal ice (920 kg/m^3). This difference is attributable to lack of clarity in the ice, which reflects the polycrystalline nature of the ice, tiny air pockets within the ice structure, as well as impurities in the tap water used. The masses of the ice spheres produced were very uniform with small standard deviation. However, because ice used to impact bridges in the field will most assuredly be less than ideal, the ice used here was considered to be of sufficient quality for determining whether ice impacts can excite the resonant acoustic modes of concrete.

For these impacts, the ideal Hertzian peak force and residence times were computed using Equation 2.8 and Equation 2.9 and then compared with the measured impact data. The calculations show that the ideal peak force is larger than the average force, which is expected, and that the steel produces the largest peak forces. The average force is noticeably less than the peak force, which is not measured directly in this experiment, because the total residence time was used to estimate the time during which a change in velocity was occurring. The expected residence times are much lower than those measured, although the measured times are similar to those reported by other researchers [81]. The ice is predicted to have a longer residence time than the steel, and this trend is also observed in the data.

A strong reason for the departure from theory for both the steel and the ice is that the dynamic, strain-rate dependent characteristics of the steel, ice, and concrete, which would influence the effective stiffness of the system, were not used in our calculations to estimate the characteristics of the Hertzian impact. Additionally, delaminations in the concrete will

Table 4.1: Estimated factors and measurement parameters from Hertzian theory and processing of recorded images for four representative impacts.

Impactor material/Concrete condition	Steel/Intact	Steel/Delam	Ice/Intact	Ice/Delam
Mass [g]	18.8	18.8	10.4	10.4
Ball Radius [mm]	8.3	8.3	14	14
Density [kg/m^3]	7850	7850	905	905
Impact Speed [m/s]	1.62	1.35	1.66	1.61
Rebound Speed [m/s]	1.03	1.11	0.33	0.14
Calculated Hertz Peak Force [N]	1,207	970	586	565
Calculated Hertz Residence Time [μs]	92	96	108	108
Measured Residence Time [μs]	48	72	88	84
Coefficient of Restitution	0.64	0.82	0.20	0.09
Energy Dissipation [mJ]	14.7	5.5	13.7	13.3
Average Force [N]	1,039	641	234	216

also influence the effective stiffness of these materials, as Hertzian theory assumes an infinite extent for the plate being impacted. Numerical modeling of the strain-rate-dependent effects would be necessary for more accurate predictions. However, the simplified Hertzian contact theory presented here does provide useful guides for the selection of impactors and materials that follow the observed trends.

Although not presented here, characterizations of impacts measured in other tests using ice spheres demonstrate that the magnitude of the force generated at the concrete surface can vary depending on whether the sphere directly strikes a rock in the concrete or instead encounters the matrix of sand and cementitious products between the rocks. The coefficients of restitution also vary widely. In some cases, the forces are sufficient to crack the ice spheres, which can also be observed in high-speed video.

The acoustic response of the concrete is visible in the spectrogram data. In both Figure 4.8 (a) and Figure 4.8 (c), which represent impacts on intact concrete, the impact of the ball bearing or ice sphere is clear, broadband, and large. The response quickly decays

as also seen in Figure 4.9 (a), and no clear resonances are visible in the spectrograms. Figure 4.8 (b) and Figure 4.8 (d), which are spectrograms of the ball bearings and ice spheres on delaminated concrete, display dominant resonant modes associated with low-frequency flexural vibrations at 1.4 and 2.5 kHz (and some additional ones for the ball bearing impact). Vibrational energy in these resonances is dissipated over a time period longer than that of the initial impact (for at least 40 ms), as has been observed in other studies of the acoustic responses of impacts [82]; the continuing resonance of the low-frequency vibrations is quite visible in Figure 4.9 (b). The similarity of the acoustic responses resulting from impacts of ball bearings and ice spheres clearly demonstrates that the ice spheres are capable of exciting the low-frequency flexural modes that are associated with concrete delaminations.

Using Equation 2.13 and Equation 2.14 for the case of a delamination that is 5 cm thick and has a diameter of 40 cm (similar to the dimensions of the observed delamination in the deck sample) gives a lower bound of 1.02 kHz and an upper bound of 2.04 kHz, which range contains the observed flexural mode of 1.4 kHz. Notably, the delamination in the concrete deck sample is not a perfectly circular plate, and this delamination is found on the edge of the slab, which will affect the observed modes; however, these calculations are generally consistent with the observed frequency response of this particular delamination.

The similarity of the acoustic responses resulting from impacts of ball bearings and ice spheres clearly demonstrate that the ice spheres are capable of exciting the low-frequency flexural modes that are associated with concrete delaminations.

4.3.2 Continuous Ice Impacts on Concrete

When ice balls are made from various molds of different sizes, thereby increasing the distribution of impactor sizes, the impactor source is naturally stochastic. The acoustic responses of the concrete resulting from continuous impacts of various sizes of ice balls on intact and delaminated concrete surface are presented in Figure 4.10. The 1.4 kHz resonance associated with the delamination is clearly visible in the multiple impacts in Figure 4.10 (b) and is absent in Figure 4.10 (a), as expected. This observed flexural frequency falls in the range of fundamental frequencies for the simply supported and clamped boundary condition as calculated in Chapter 2. The ice sphere delivery rate was above 10 impactors per second.

This was achieved by emptying a container of different-sized ice spheres above a funnel leading to a 1.5-m plastic tube directed towards the impact location. Possible bounces were not removed from the data.

For this demonstration, signal processing of the response was performed by first finding impact times. Then, at each impact time, a spectrogram was computed. Examples of individual spectrograms for intact and delaminated impacts are shown in Figure 4.12 (a) and Figure 4.12 (b). To extract features from each spectrogram, the maximum-energy frequency was found, chosen empirically after 3.7 ms had passed. The delay was used to ignore the direct impact sound and analyze the subsequent response from the impact. A scaled amplitude was computed by calculating a sum of the spectrogram power terms at the maximum energy frequency during the first 3.7 ms to account for different impact strengths [83].

Estimation results on the intact and delaminated sequences from this procedure are drawn in a three-dimensional plot as shown in Figure 4.13 [84]. The differences between the intact and delaminated sections are clearly shown even though a stochastic source was used. The delaminated sections are characterized by lower maximum frequency, higher scaled amplitude, and more negative decay constants, which result from exciting a low-frequency flexural mode that subsequently resonates energy for some tens of milliseconds after the impact. Points P1 and P2 in the data in Figure 4.13 seem to imply that the energy is

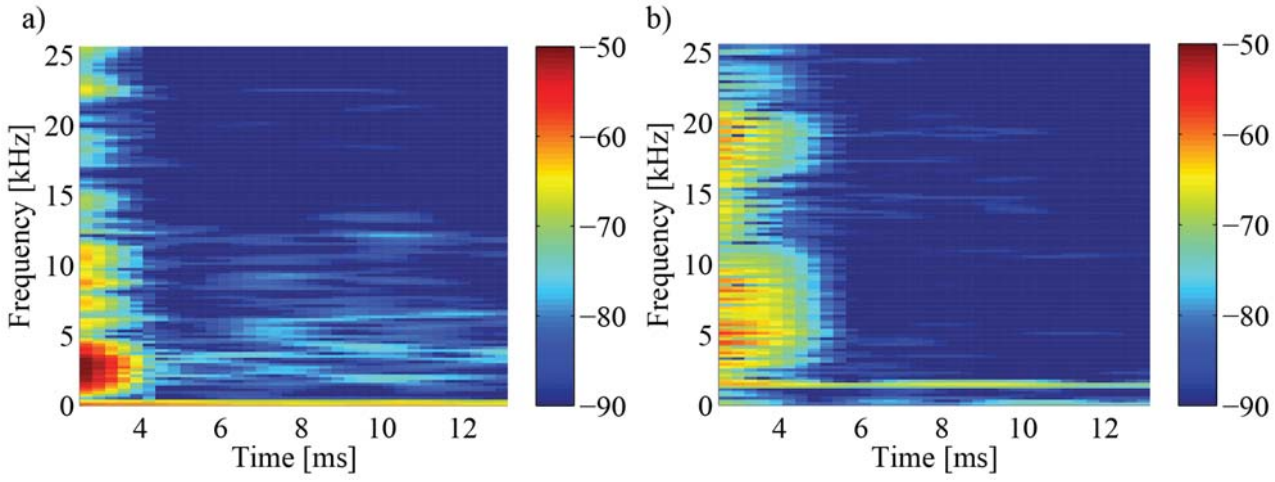

Figure 4.12: Sub-spectrogram of single ice sphere impacts from Figure 4.10 on (a) intact and (b) delaminated areas of concrete. The scale is in dB.

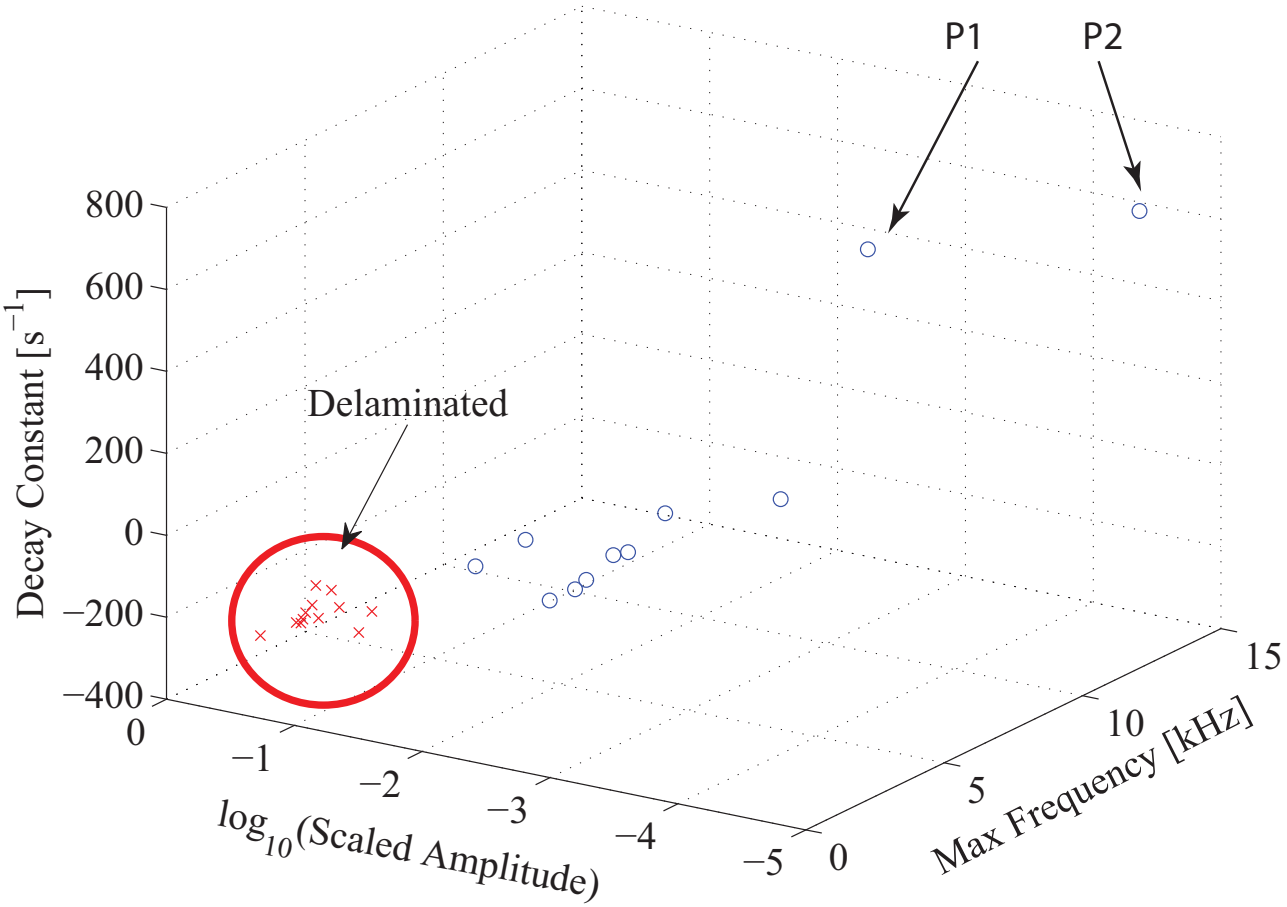

Figure 4.13: Three-dimensional plot of the features extracted from the continuous ice impact data on intact and delaminated concrete sections. The features of the delaminated concrete are clearly separated from those of the intact area.

increasing for their impacts on the intact concrete. While these data sets were collected from relatively small areas of concrete in the laboratory, they clearly show how an unsupervised signal processing and classification framework [85] could be used to interpret impact-echo data using a stochastic impact source.

These analyses show that ice spheres can be effectively used as impactors for impact-echo testing of concrete bridge decks. We have also observed that non-spherical ice can be used to excite acoustic modes in concrete, though impact orientation appears to be important (data not shown). More development and characterization will be required to fully deploy the technique in the field. Multiple impacts at similar locations could be advantageous

to increase the classification power and spatially correlate the results. Additionally, signal processing to account for potentially noisy environments will also be required [85].

4.4 Conclusion

This study demonstrates that ice spheres can be effectively used to produce impacts that are comparable to those of steel ball bearings for impact-echo testing of concrete bridge decks. Ice spheres are attractive impactors for detecting delaminations because they are disposable and environmentally friendly, they would melt away quickly when applied during warm seasons, and they would have minimal adverse effects on the safety of the traveling public. In combination with air-coupled acoustic response measurements and minimally-supervised signal processing techniques [85], this method of excitation could be used to perform automated deck condition assessments, eliminating subjectivity and greatly increasing data collection speeds.

Chapter 5

Comparison of Impactors

In this chapter, the acoustic responses produced by various impactors such as steel balls, separated chain links, and ice balls of varying sizes are compared. Air-coupled measurement was used in combination with these impactors to detect shallow delaminations in concrete. The goal of this experiment was to compare the acoustic responses of these impactors for the detection of shallow delaminations in concrete.

5.1 Testing Material and Experimental Method

The concrete slab shown in Figure 4.1 was used for the experiment. Three different sizes of steel ball bearings, steel chain links, and ice balls were used as impactors and are shown in Figure 5.1. The mass and radius of each impactor are listed in Table 5.1. The chain links used were separated from chains that produced clear ringing sounds on intact concrete surface and hollow sounds on delaminated concrete surface and were thus good choices as impactors [15]. Ice balls were fabricated by freezing deionized water in two-piece ice trays having spherical molds with diameters of 26 mm, 28 mm, and 32 mm in a standard freezer (-16 to $-9\,^{\circ}$C). The tests were performed using these impactors at the representative intact and delaminated test locations.

For mapping the entire deck slab, 35 different test locations were marked on the slab based on a preliminary chain drag. A steel chain of link size 54 mm (7.5-mm inner diameter) was used for this purpose. Test locations were marked as relatively intact points when a clear ringing sound was heard, while for the hollow sound the test locations were marked as delaminated points. Different impactors were then dropped on the marked test locations, and acoustic responses were recorded.

Figure 5.1: Photographs of steel chain links, steel ball bearings, and ice balls of three different sizes used as impactors.

Table 5.1: Radius and mass of impactors

Impactor	Mass [g]	Radius [mm]
Steel Ball 1	0.44	1.95
Steel Ball 2	1.05	3.15
Steel Ball 3	18.8	8.3
Ice Ball 1	10	13
Ice Ball 2	10.4	14
Ice Ball 3	15.9	16
Chain link 1 (size: 24 mm)	2.1	3
Chain link 2 (size: 38 mm)	4.7	7.5
Chain link 3 (size: 54 mm)	61.6	7.5

To release steel balls and chain links consistently, an APW electromagnet EM075-6-122 (19.05-mm diameter, 6 VDC) was mounted 2.0 m above the impact point on the concrete slab as shown in Figure 5.2. For dropping ice balls consistently, a circular diaphragm aperture as previously described was mounted at the same height above the impact point. To impact test locations across the slab, a movable steel frame as shown in Figure 5.2 was used. The

center rod of the frame could move in the X direction, while the C-frame could move in the Y direction.

The acoustic data were recorded using the same microphone as described in Chapter 4 and post-processed in MATLAB to produce spectrograms of impacts. A sliding 512-point Hamming window with 500 overlap points was used to compute the 512-point periodogram of the acoustic data, and the power spectral density was estimated.

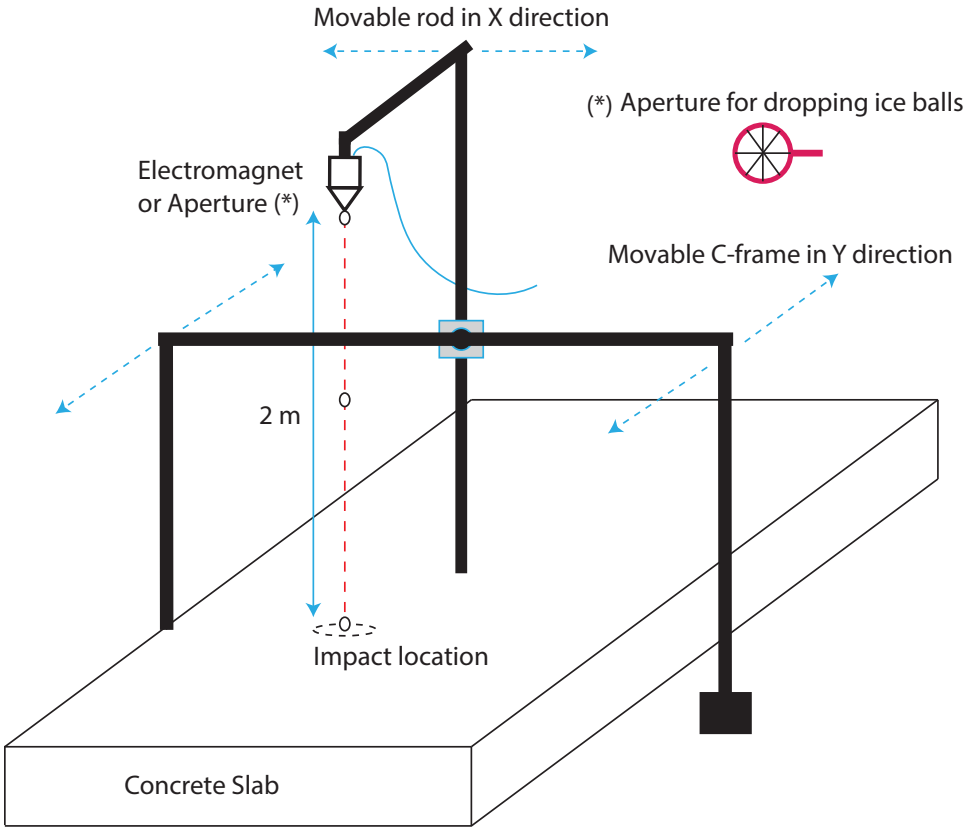

Figure 5.2: Schematic of movable steel frame over deck sample with attached electromagnet for dropping steel balls or chain links and aperture for dropping ice balls

5.2 Results and Discussion

Tests were performed on relatively intact and delaminated points on the sample deck slab. The intact test point was close to the center of the slab, while the delaminated spot was very close to the edge of the concrete (70 mm). Using Equation 2.13 and Equation 2.14 for the case of a delamination that is 50-mm thick and has a diameter of 400 mm (similar to the dimensions of the observed delamination on the deck sample), a lower bound of 1.02 kHz and an upper bound of 2.04 kHz were computed. The delamination in the concrete deck sample is not a perfectly circular plate, and this delamination is found on the edge of the slab, which will affect the observed modes; however, these calculations are generally consistent with the observed frequency response of this particular delamination. A comparison of acoustic responses of various impactors at these representative test locations was performed.

5.2.1 Steel Ball as an Impactor

The acoustic spectrograms for the initial impacts of steel ball 1 on intact and delaminated surface are shown in Figure 5.3. The power spectral densities computed at intact and delaminated test points are presented in Figure 5.6. The observed peak frequency (with maximum power) is 1.363 kHz and is readily apparent in the power spectral density shown in Figure 5.6. The acoustic spectrograms of initial impacts of steel ball 2 and steel ball 3 are shown in Figure 5.4 and Figure 5.5, respectively. Figure 5.7 and Figure 5.8 represent the power spectral densities at intact and delaminated concrete surface using steel ball 2 and steel ball 3 respectively.

The peak frequency for the steel ball 3 impact is observed at 9.8 kHz. This is the full thickness mode frequency for the test slab. The same peak frequency is not observed for the case of steel balls 1 and 2. The size and mass of the ball controls the frequency range that is excited, and the diameter of the ball generally is inversely proportional to the maximum excitable frequency [86]. The results also show that the full thickness mode frequencies are affected by the ball size, but the flexural mode low frequencies are independent of the ball size. Even though different sized steel balls were used in the experiment, the power spectral densities indicate that the flexural mode excitation frequency is consistent and is approximately 1.36 kHz for the tested delaminated point. The observed mode of 1.36 kHz

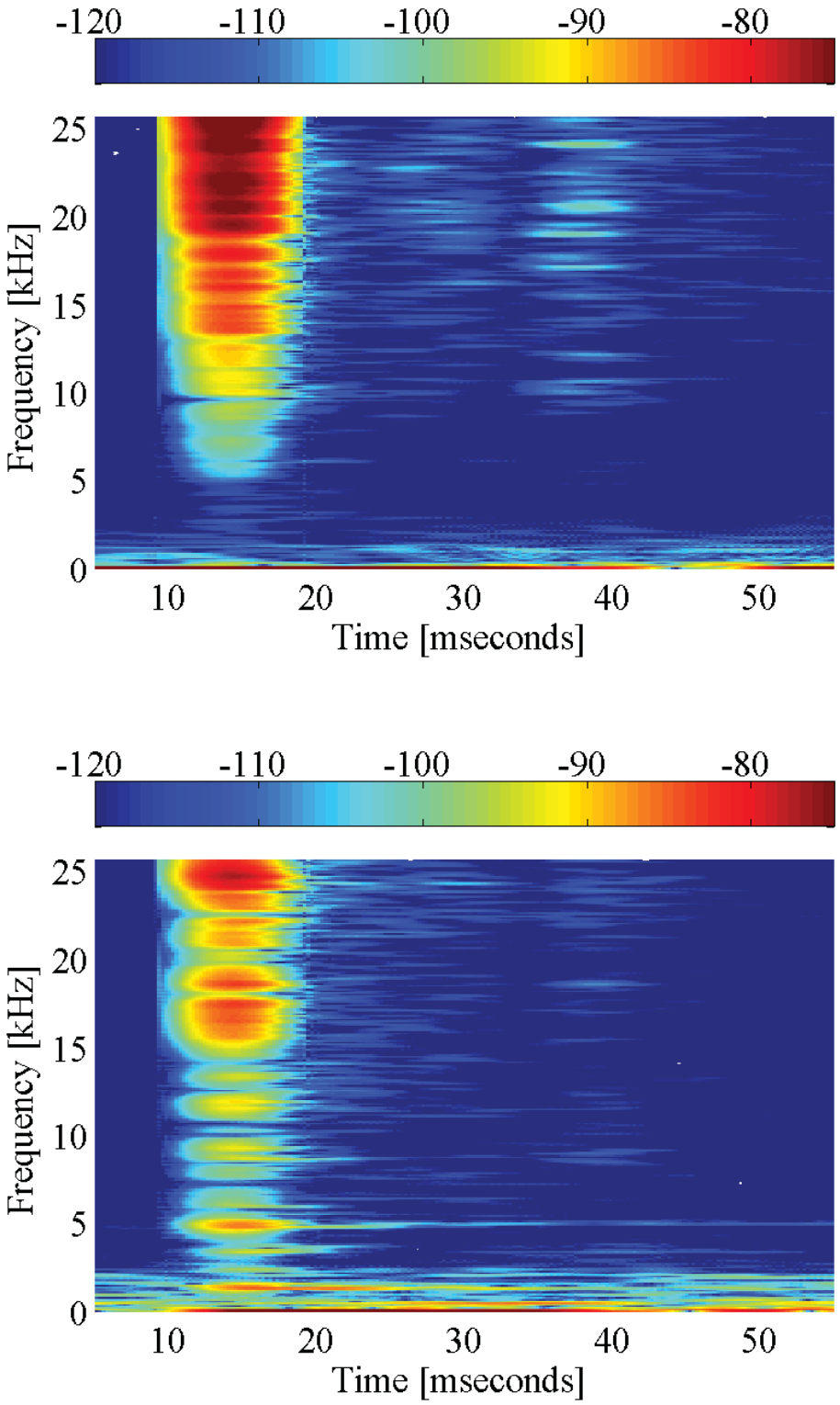

Figure 5.3: Spectrograms of acoustic data recorded using steel ball 1. The top spectrogram was recorded over intact concrete, while the bottom spectrogram was recorded over a delamination. The color bar indicates the sound level in dB. The low-frequency acoustic modes associated with the delamination are readily apparent in the bottom spectrogram.

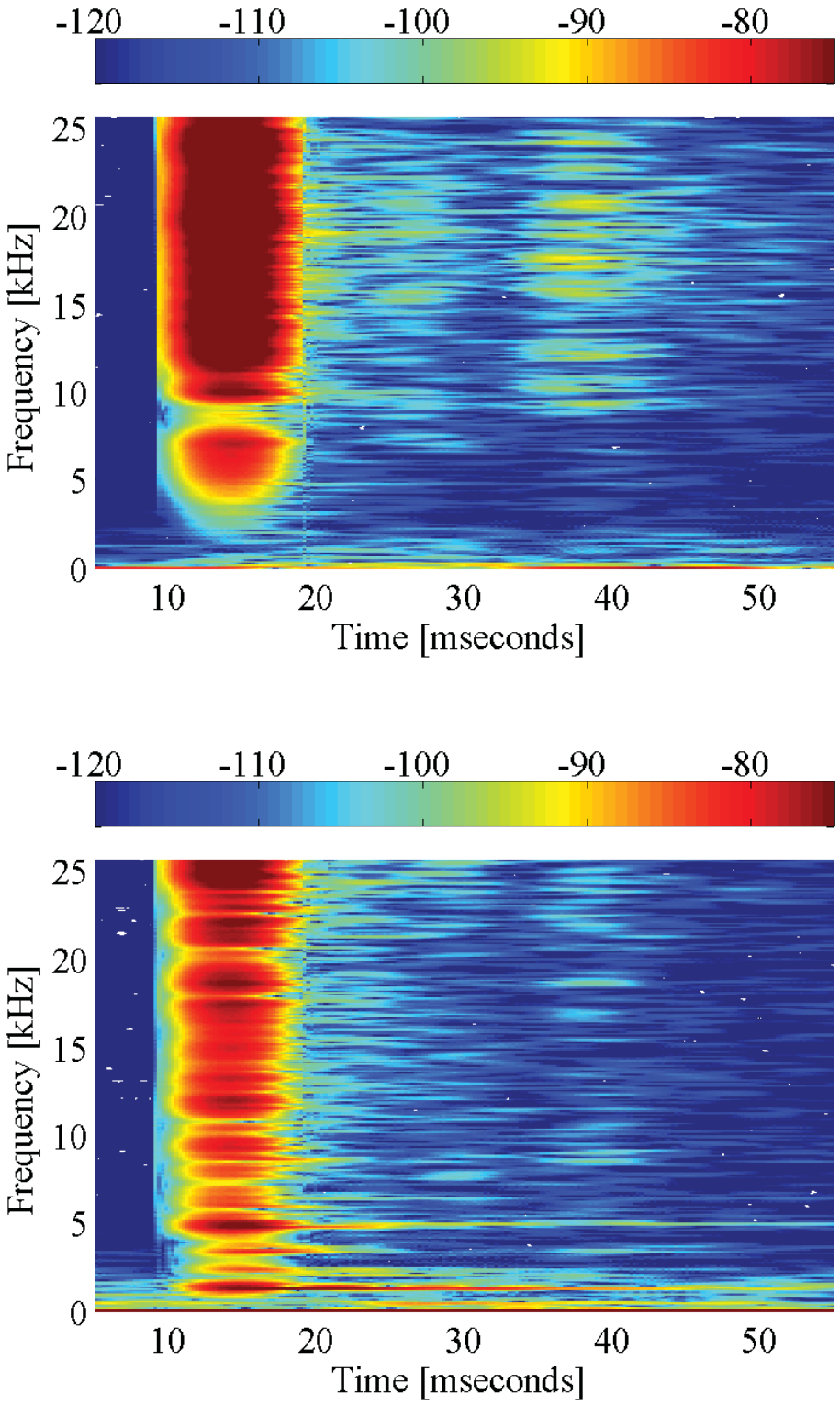

Figure 5.4: Spectrograms of acoustic data recorded using steel ball 2. The top spectrogram was recorded over intact concrete, while the bottom spectrogram was recorded over a delamination. The color bar indicates the sound level in dB. The low-frequency acoustic modes associated with the delamination are readily apparent in the bottom spectrogram.

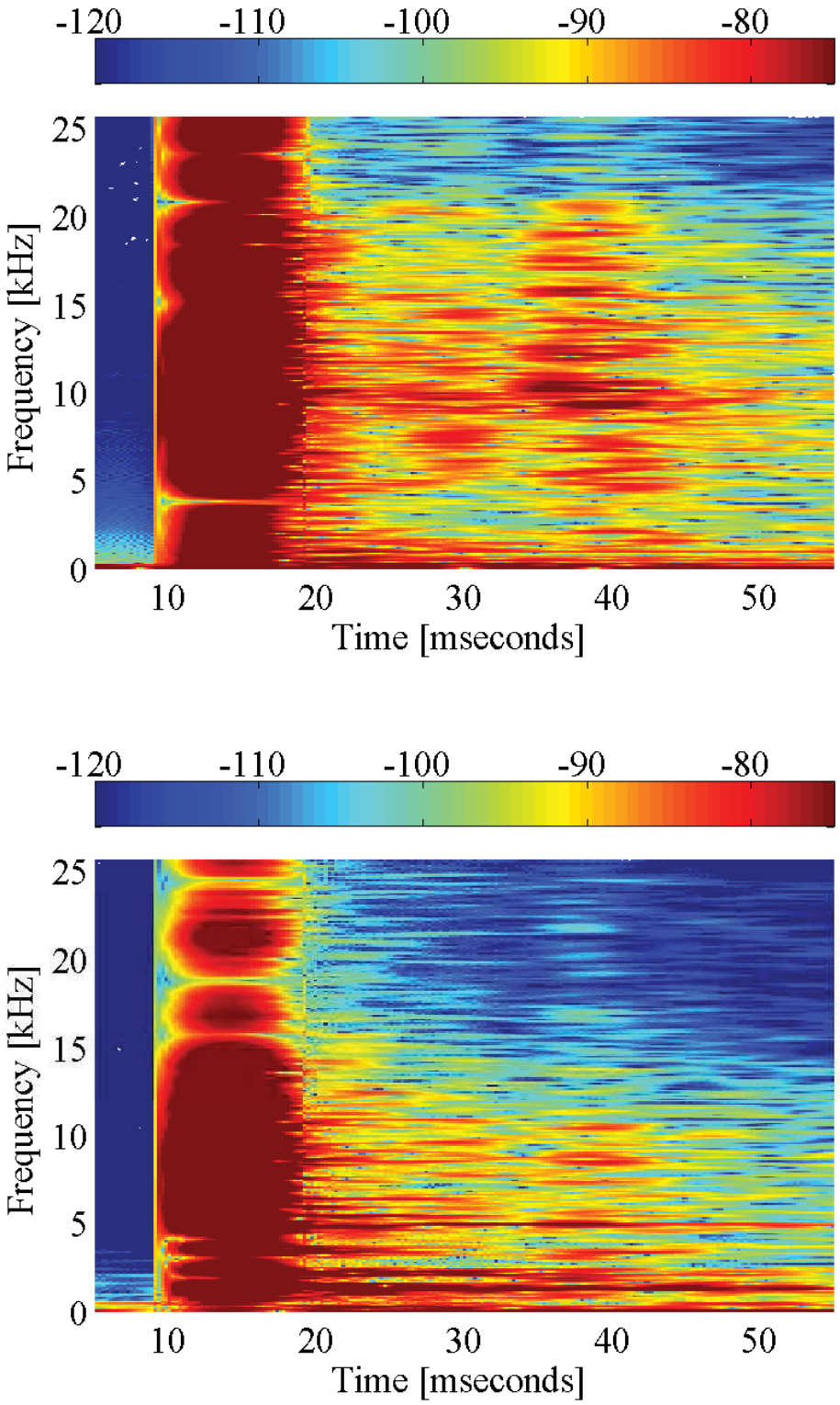

Figure 5.5: Spectrograms of acoustic data recorded using steel ball 3. The top spectrogram was recorded over intact concrete, while the bottom spectrogram was recorded over a delamination. The color bar indicates the sound level in dB. The low-frequency acoustic modes associated with the delamination are readily apparent in the bottom spectrogram.

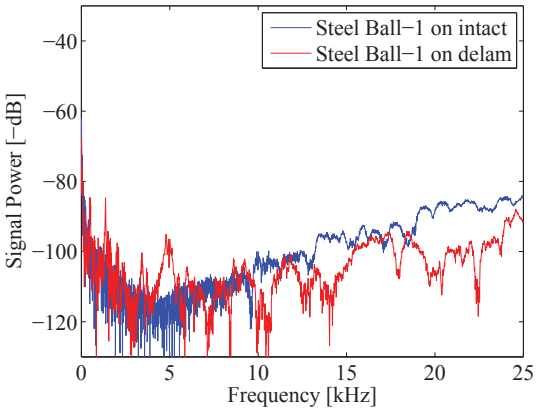

Figure 5.6: Power spectral density of an impact using steel ball 1 on intact and delaminated concrete surface. The peak frequency associated with flexural mode of delamination is 1.363 kHz.

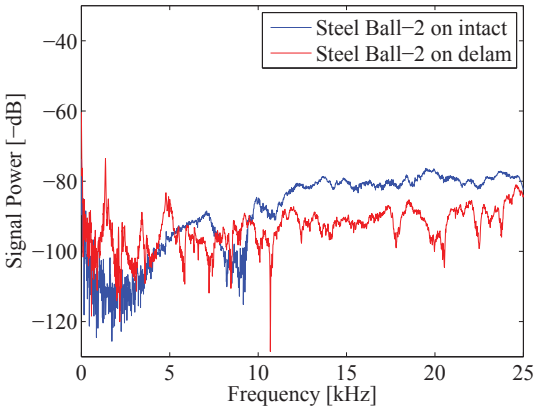

Figure 5.7: Power spectral density of an impact using steel ball 2 on intact and delaminated concrete surface. The peak frequency associated with flexural mode of delamination is 1.363 kHz.

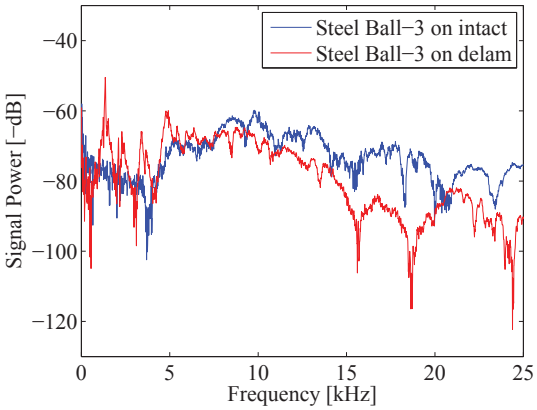

Figure 5.8: Power spectral density of an impact using steel ball 3 on intact and delaminated concrete surface. The peak frequency associated with flexural mode of delamination is 1.35 kHz.

falls in the range of estimated upper and lower bound frequencies for the shallow delamination as mentioned previously.

5.2.2 Chain Link as an Impactor

The acoustic spectrograms for the impacts of chain link 1, chain link 2, and chain link 3 on the intact and delaminated test locations with their power spectral densities are presented in Figure 5.9, Figure 5.10, and Figure 5.11, respectively. Both chain link 1 and chain link 2 used in the experimentation were not intact and had slits in them, while chain link 3 was intact. This can be observed in Figure 5.1. The slits in chain links 1 and 2 contribute to the ringing of the chain links themselves at lower frequencies. Figure 5.9(c) shows the ringing modes of chain link 1 indicated as frequency peaks at 5.5 kHz, 6.8 kHz, 8.7 kHz, 11.4 kHz, 14.8 kHz, and 17.6 kHz. The similar frequency modes associated with ringing of the chain link 1 are visible in Figure 5.9(d) with low-frequency excitation. The low frequency peak of 1.375 kHz associated with the delamination as observed in Figure 5.9(d) is absent in Figure 5.9(c) for the intact location. Similar effects are observed for chain link 2 in Figure 5.10 with a frequency peak at 1.363 kHz for the delamination.

Unlike chain links 1 and 2, the intact chain link 3 did not produce the ringing modes of the link itself at lower frequencies. Both Figure 5.11(c) and Figure 5.11(d) indicate a ringing mode frequency of 14.6 kHz of the link itself for intact and delaminated concrete. A low-frequency peak of 1.344 kHz associated with a shallow delamination is readily apparent in Figure 5.11(d).

5.2.3 Ice ball as an Impactor

The spectrogram analysis of the acoustic data measured at intact and delaminated locations on the concrete surface using ice balls 1, 2, and 3 are shown in Figure 5.12, Figure 5.13, and Figure 5.14, respectively. Figure 5.15, Figure 5.16, and Figure 5.17 present the power spectral densities for the same. Ice balls 1, 2, and 3 excite the shallow delamination frequencies of 1.35 kHz, 1.34 kHz, and 1.35 kHz, respectively. The flexural mode frequency excitation for all the three sizes is very much consistent and is less affected by the noise.

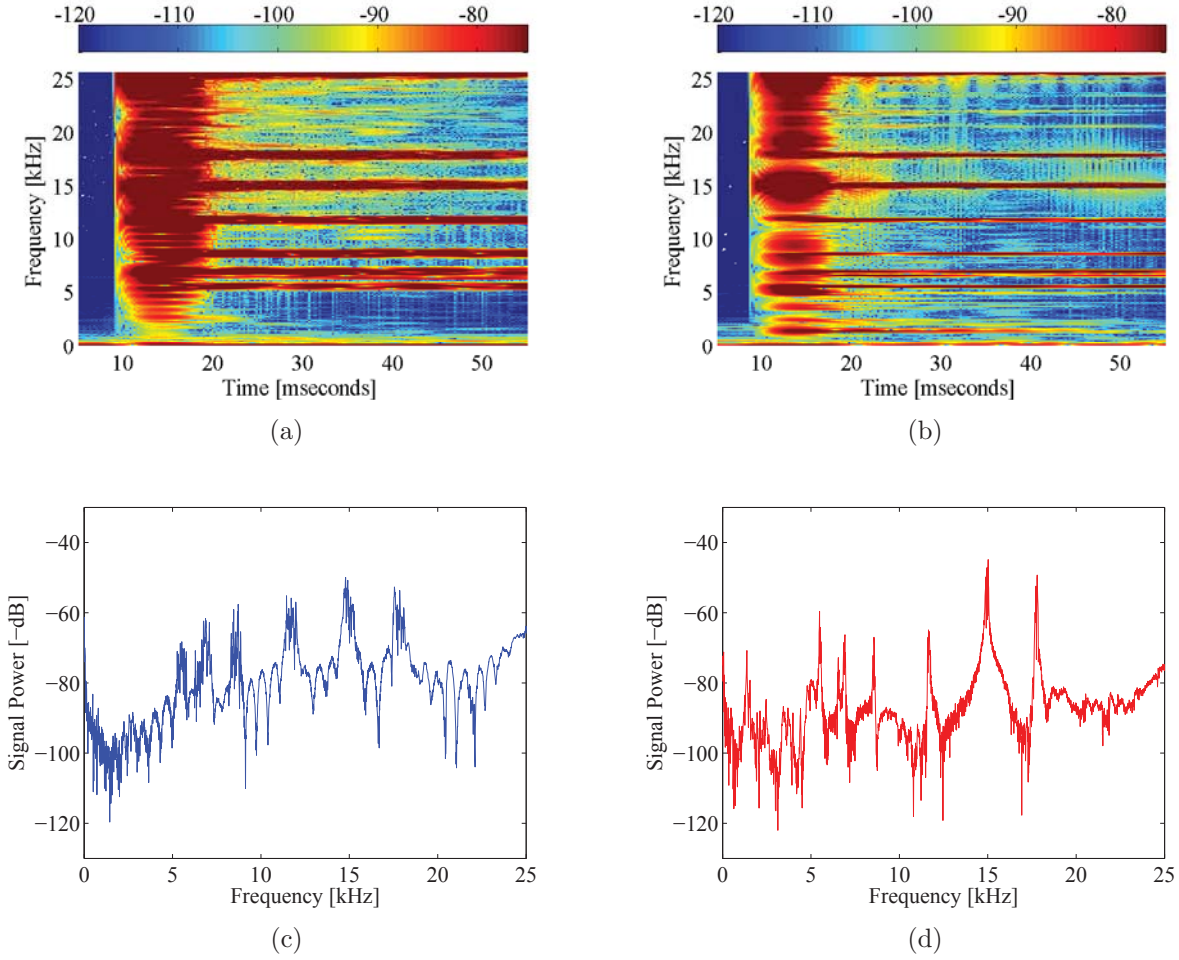

Figure 5.9: Acoustic responses recorded over intact and delaminated concrete surface using chain link 1 as an impactor. The color bar indicates the sound level in dB. The low frequency acoustic modes of 1.375 kHz associated with the shallow delamination are clearly visible. (a) and (c): Spectrogram and power spectral density of acoustic data recorded over intact concrete surface. (b) and (d): Spectrogram and power spectral density of acoustic data recorded over delaminated concrete surface.

Unfortunately, the size of ice balls used in the experiment were not able to excite the full thickness mode frequency of the test slab. Also, cracking of the ice balls was observed after initial impact, which indicates that much of the impact energy is dissipated in the cracking process. This was also observed by other researchers [68, 69].

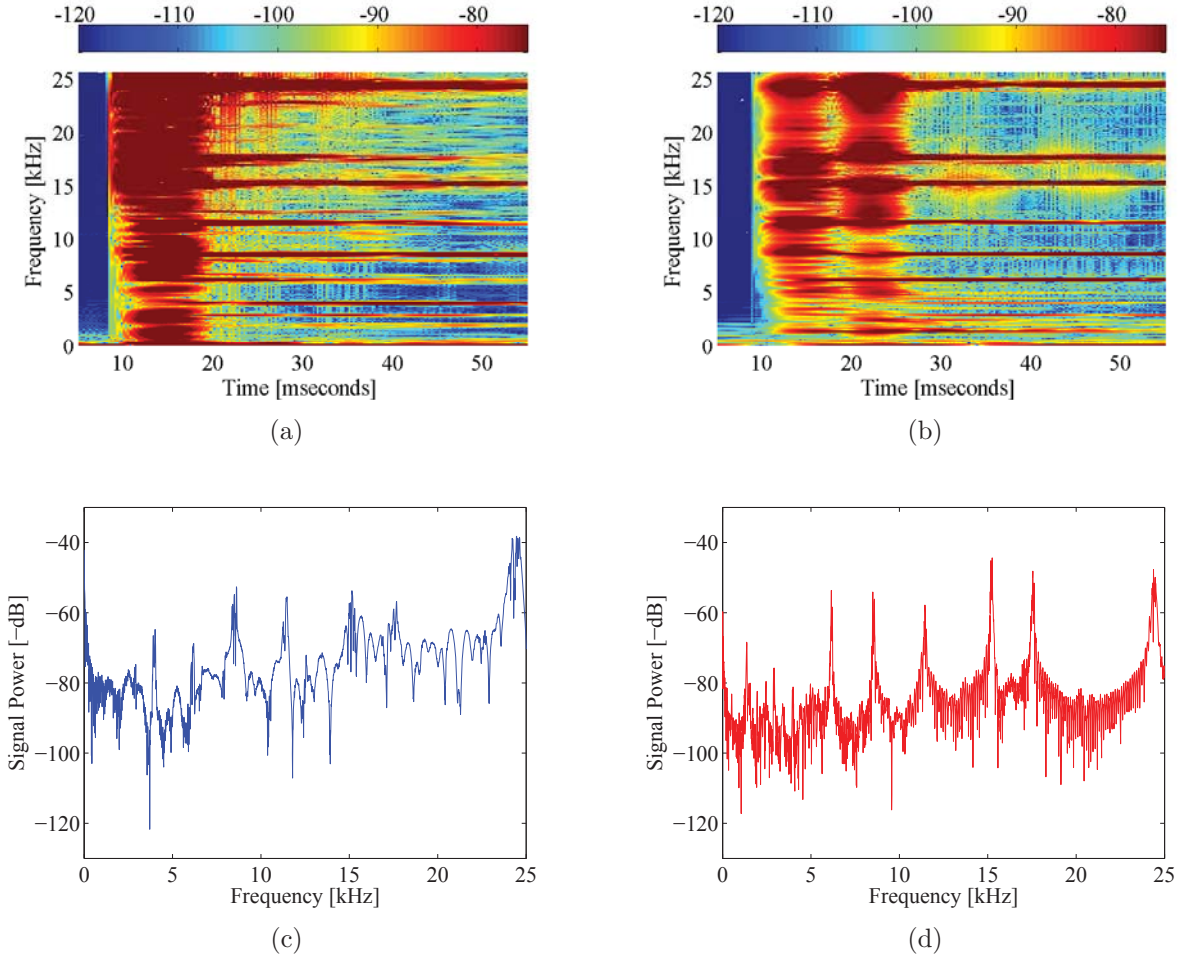

Figure 5.10: Acoustic responses recorded over intact and delaminated concrete surface using chain link 2 as an impactor. The color bar indicates the sound level in dB. The low frequency acoustic modes of 1.363 kHz associated with the shallow delamination are clearly visible. (a) and (c): Spectrogram and power spectral density of acoustic data recorded over intact concrete surface. (b) and (d): Spectrogram and power spectral density of acoustic data recorded over delaminated concrete surface.

5.2.4 Three-Dimensional Plotting for Steel Balls and Ice Balls

The data collected at 35 different test locations on the slab were analyzed using MATLAB. To extract features from each spectrogram at different locations, the frequency with maximum energy was computed after a delay of 24 ms for impacts of steel balls and ice balls and after 36 ms for chain link impacts (to filter out the initial impact sound). An exponential fitting function was used to fit data at these frequency values, and then the

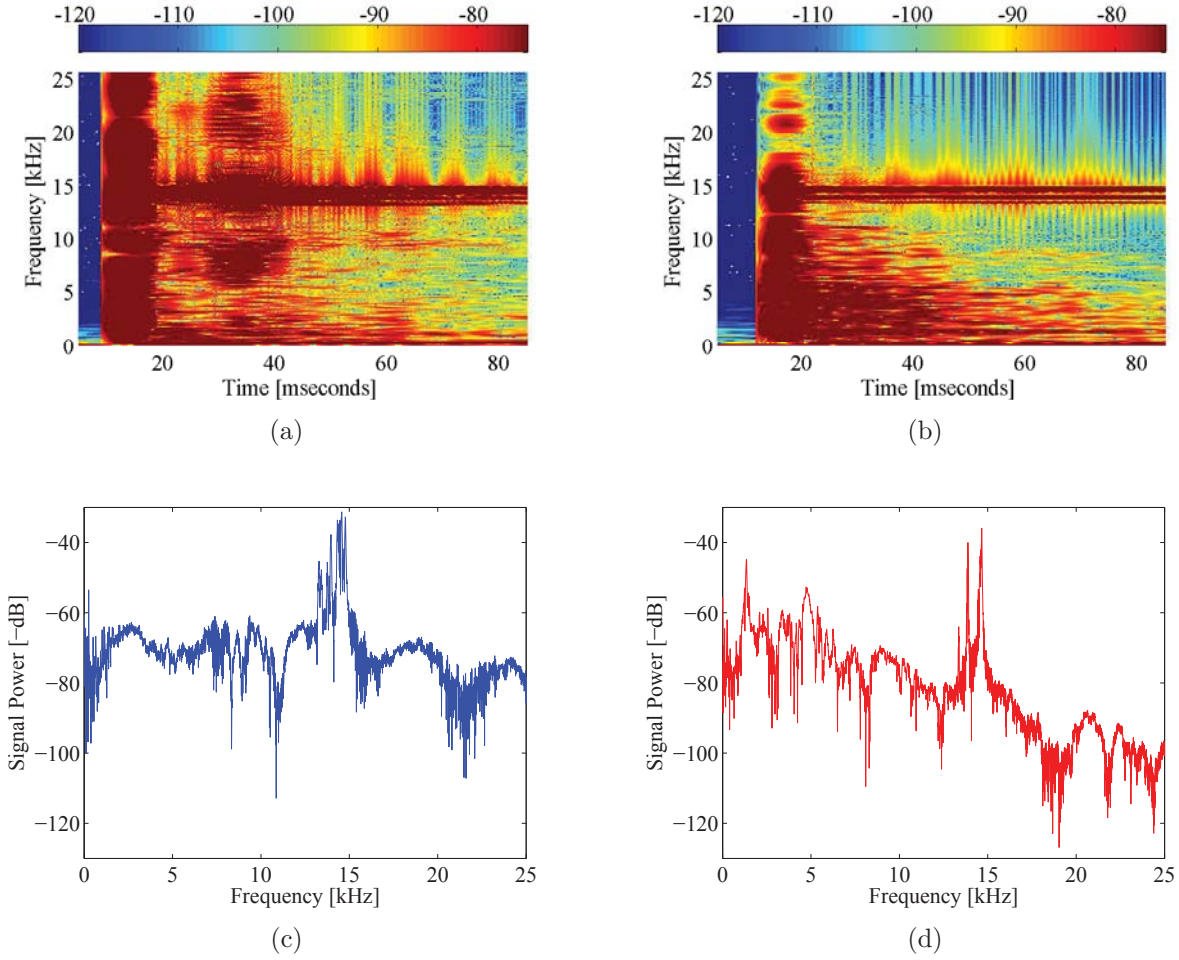

Figure 5.11: Acoustic responses recorded over intact and delaminated concrete surface using chain link 3 as an impactor. The color bar indicates the sound level in dB. The low frequency acoustic modes of 1.344 kHz associated with the shallow delamination are clearly visible. (a) and (c): Spectrogram and power spectral density of acoustic data recorded over intact concrete surface. (b) and (d): Spectrogram and power spectral density of acoustic data recorded over delaminated concrete surface.

decay constants were computed from the exponential fit. This decay time represents the time taken to dissipate the energy in any resonant modes at the post-impact frequency with maximum energy. Figure 5.18, Figure 5.19, and Figure 5.20 show the three-dimensional plot of estimated results for the case of steel ball 3, chain link 3, and ice ball 3, respectively. In Figure 5.18 the intact and delaminated points are clearly separated. The delaminated sections are characterized by lower maximum energy frequency, more negative decay constant

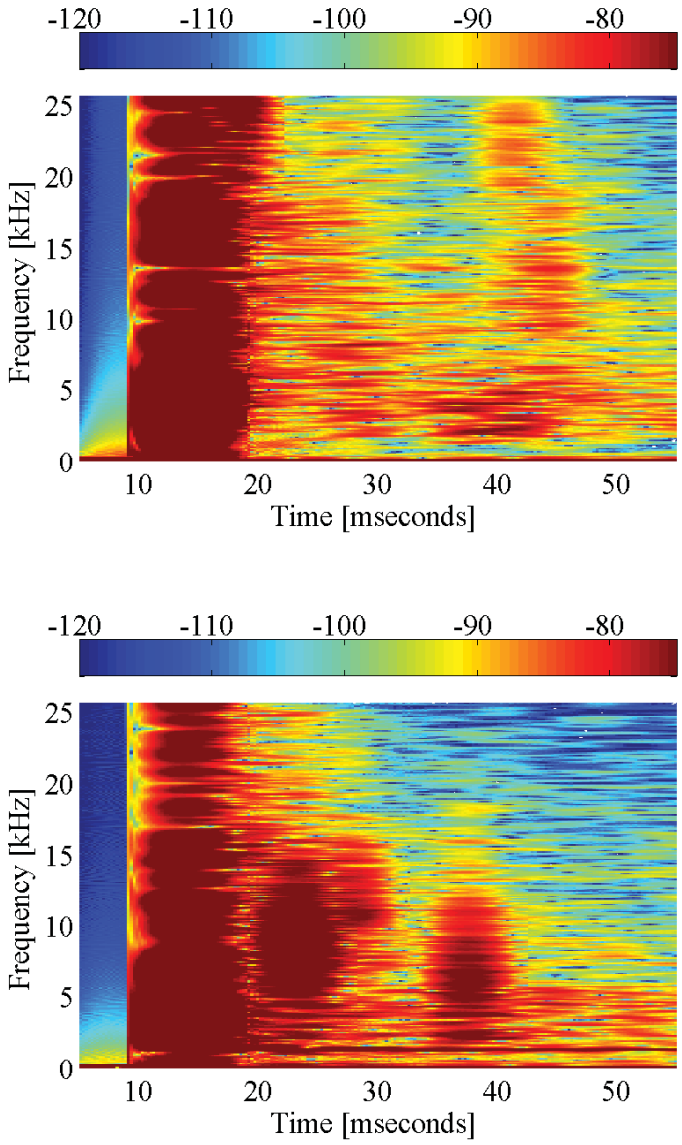

Figure 5.12: Spectrograms of acoustic data recorded using ice ball 1. The top spectrogram was recorded over intact concrete, while the bottom spectrogram was recorded over a delamination. The color bar indicates the sound level in dB. The low-frequency acoustic modes associated with the delamination are readily apparent in the bottom spectrogram.

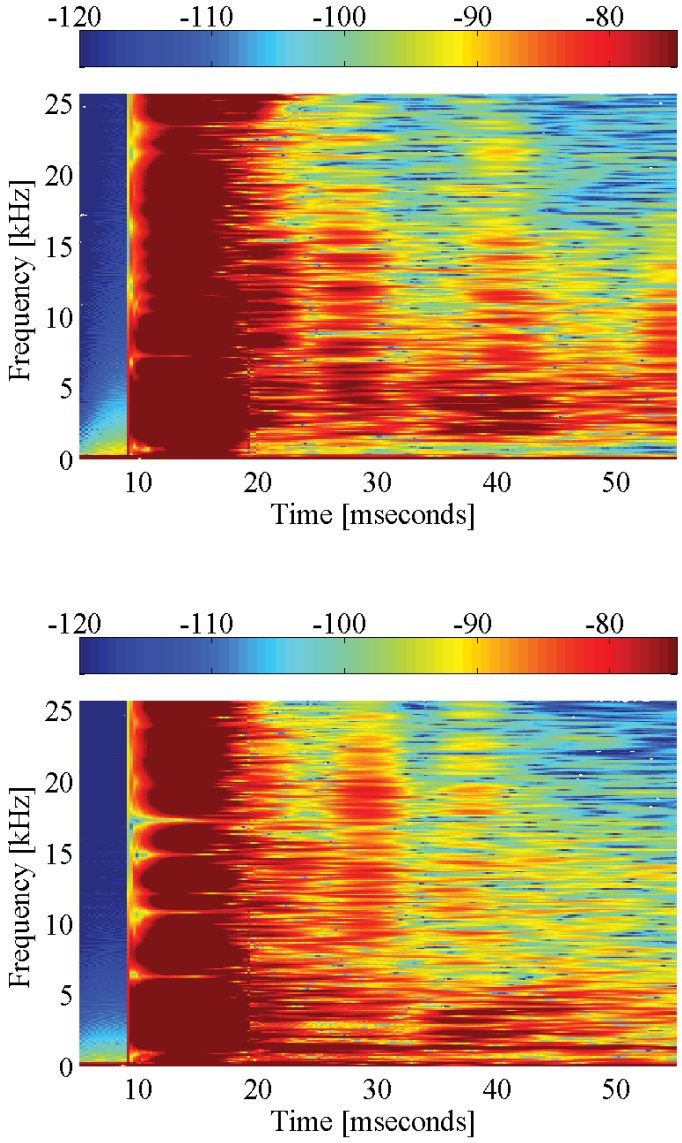

Figure 5.13: Spectrograms of acoustic data recorded using ice ball 2. The top spectrogram was recorded over intact concrete, while the bottom spectrogram was recorded over a delamination. The color bar indicates the sound level in dB. The low-frequency acoustic modes associated with the delamination are readily apparent in the bottom spectrogram.

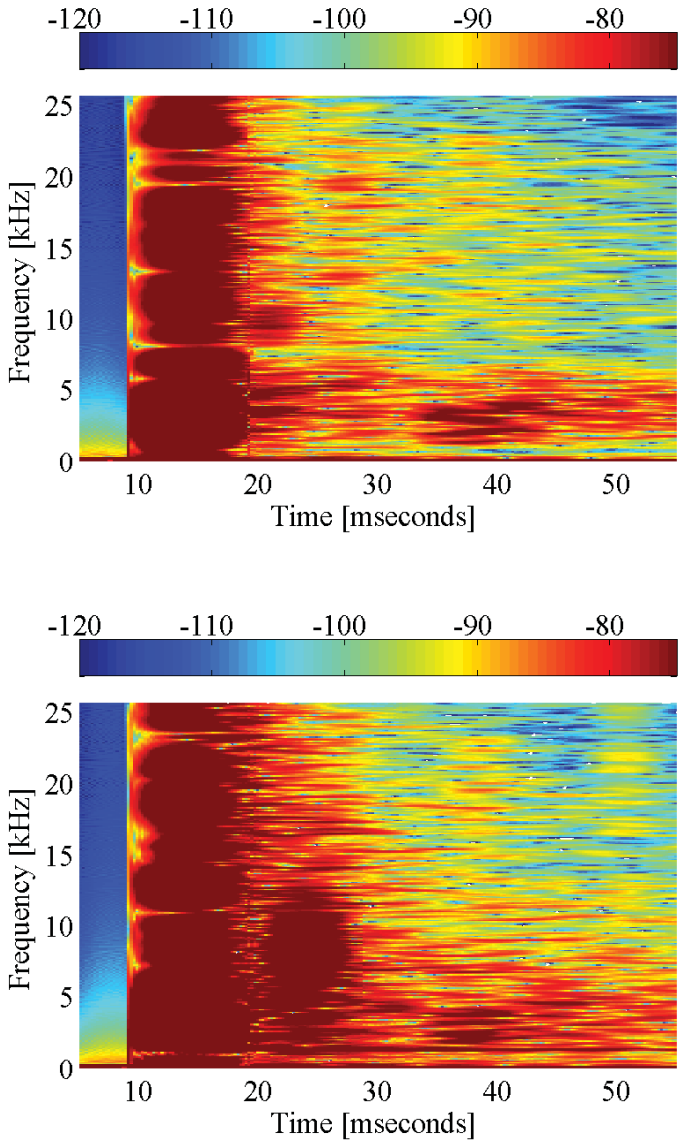

Figure 5.14: Spectrograms of acoustic data recorded using ice ball 3. The top spectrogram was recorded over intact concrete, while the bottom spectrogram was recorded over a delamination. The color bar indicates the sound level in dB. The low-frequency acoustic modes associated with the delamination are readily apparent in the bottom spectrogram.

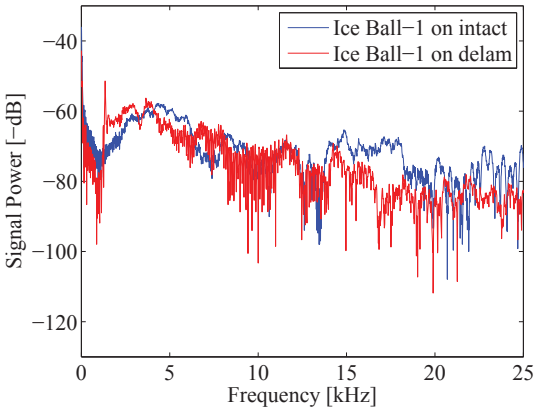

Figure 5.15: Power spectral density of an impact of an ice ball 1 on intact and delaminated concrete surface. The peak frequency associated with flexural mode of delamination is 1.35 kHz.

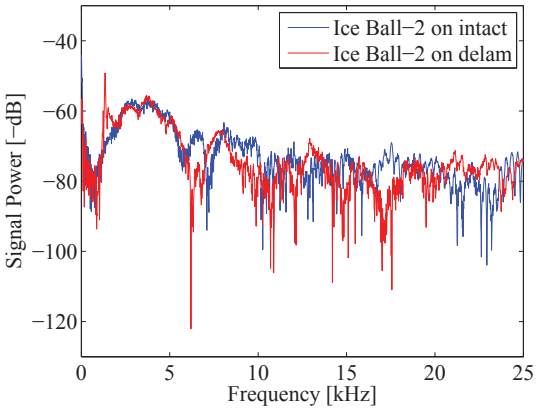

Figure 5.16: Power spectral density of an impact of an ice ball 2 on intact and delaminated concrete surface. The peak frequency associated with flexural mode of delamination is 1.34 kHz.

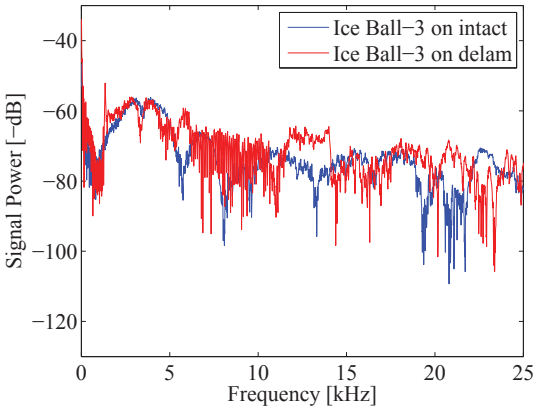

Figure 5.17: Power spectral density of an impact of an ice ball 3 on intact and delaminated concrete surface. The peak frequency associated with flexural mode of delamination is 1.35 kHz.

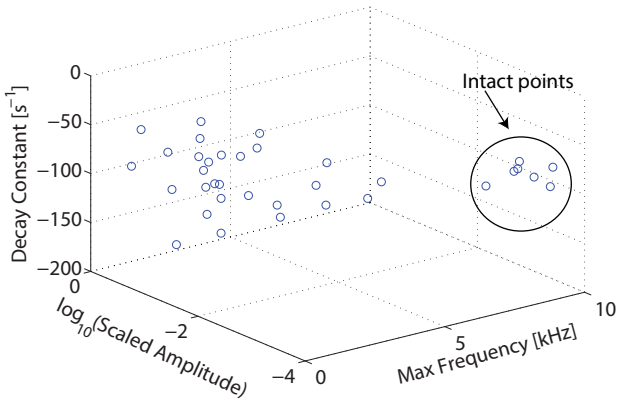

Figure 5.18: 3-D plot of the features extracted from the acoustic data obtained on 35 test locations on the slab using steel ball 3. The features of the delaminated concrete are clearly separated from those of the intact area.

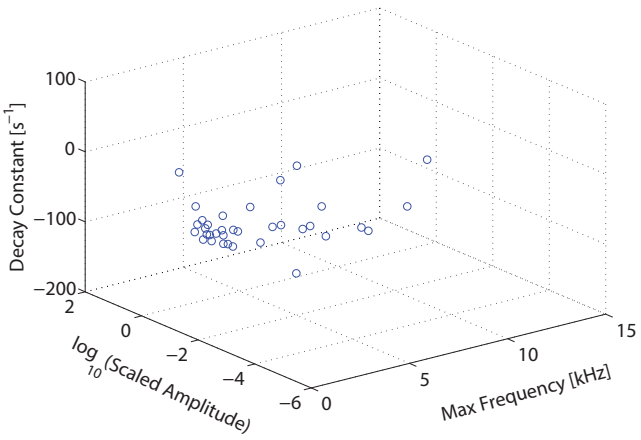

Figure 5.19: 3-D plot of the features extracted from the acoustic data obtained on 35 test locations on the slab using chain link 3. The features of the delaminated concrete are grouped well.

and higher scaled amplitudes. For the data using chain link 3, in Figure 5.19 low frequencies associated with shallow delaminated are grouped well. However, in Figure 5.20 the estimated features are not clearly separated. Since most of the ice balls were dropped from the height of 2 m cracked upon impact (observed in the high-speed video of the impact), the impact force generated at impact is clearly sufficient to break the ice ball. This behavior was observed to be highly variable at the different test locations.

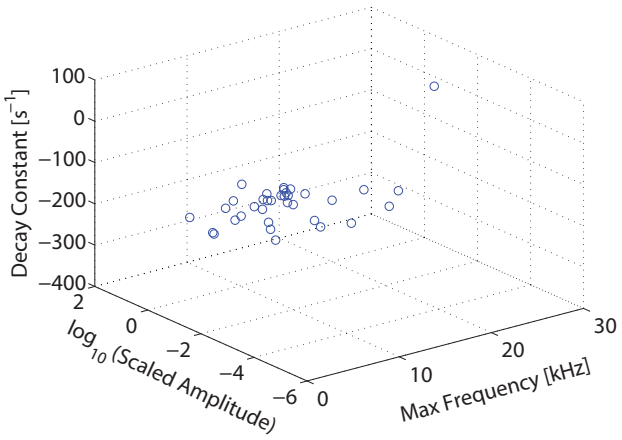

Figure 5.20: 3-D plot of the features extracted from the acoustic data obtained on 35 test locations on the slab using ice ball 3. The features of the delaminated concrete are not separated from those of the intact area.

5.2.5 Two-Dimensional Frequency Mapping

Two-dimensional frequency mapping is a plot of frequencies with maximum power across a rectangular grid and has been shown to be useful for data representation in impact-echo measurements [19]. The frequency map is constructed using contour plots in MATLAB. Figure 5.21(a), Figure 5.21(b), and Figure 5.21(c) show the frequency maps obtained using steel ball 3, chain link 3, and ice ball 3, respectively. The data points used to construct these maps were based on the preliminary chain-drag test performed across the sample deck slab. The lower frequencies corresponding to flexural modes are indicated by warmer colors, while the higher frequencies with maximum power are indicated by cooler colors in the plots.

Frequency maps shown in Figure 5.21 effectively indicate the presence of shallow delaminations across the sample deck slab. The frequency maps obtained for all three impactors show that most of the slab is covered with shallow delaminations. The frequency maps produced using steel ball and chain link match well in terms of the presence of shallow delaminations and indicate few intact locations on the sample deck slab. The blue-colored region on the top left portion of the slab as shown in Figure 5.21(c) indicates high-frequency peak greater than 15 kHz. Such high frequencies at the same locations were not observed in Figure 5.21(a) and Figure 5.21(b). Also, the spread of the shallow delaminated locations

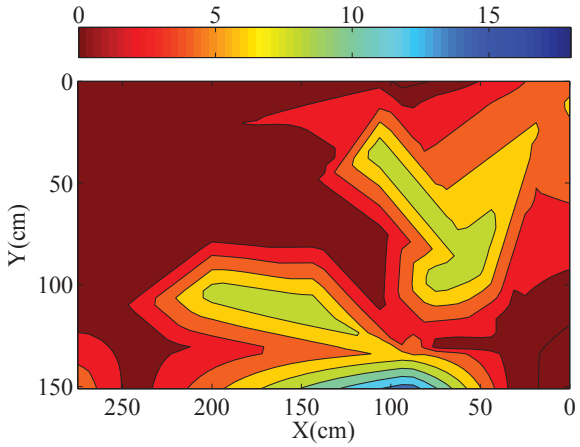

(a) Frequency map using steel ball 3 as an impactor

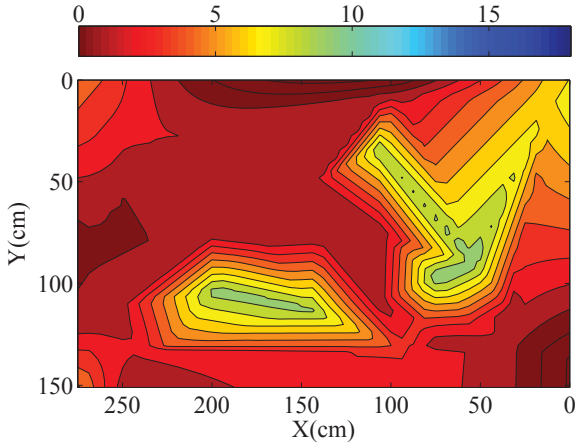

(b) Frequency map using chain link 3 as an impactor

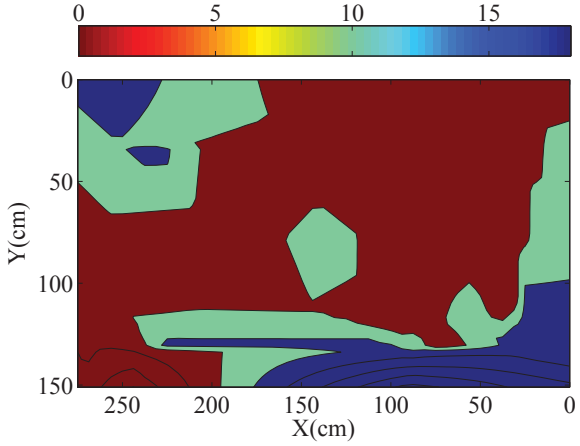

(c) Frequency map using ice ball 3 as an impactor

Figure 5.21: Frequency maps using contour plot in MATLAB showing the frequencies with maximum power obtained from air-coupled impact measurements at different locations on the sample deck slab. The color bar represents frequency values in kHz.

observed in Figure 5.21(c) is relatively lower compared to the frequency maps shown in Figure 5.21(a) and Figure 5.21(b).

5.3 Conclusion

The results obtained for the low-frequency flexural excitations using the different impactors are listed in Table 5.2. These indicate that low-frequency flexural vibrations can be excited by a variety of impactors. However, the high-frequency responses are much more dependent on different impactors. To use ice balls for detection, further development and optimization will be required to deploy the technique in the field.

The frequency maps presented indicate that most of the sample deck slab is covered with shallow delaminations. The frequency maps produced using steel ball 3 and chain link 3 agree well at most of the test locations. Out of 35 tested locations on the sample deck slab, steel ball and chain link detected shallow delaminations at 29 locations, while ice ball was able to detect shallow delaminations at 19 tested locations.

Table 5.2: Flexural mode frequencies obtained using impactors with varying sizes

Impactor	Flexural Frequency (kHz)
Steel Ball 1	1.363
Steel Ball 2	1.363
Steel Ball 3	1.35
Ice Ball 1	1.35
Ice Ball 2	1.337
Ice Ball 3	1.35
Chain Link 1	1.375
Chain Link 2	1.363
Chain Link 3	1.344

Chapter 6

Conclusion

Impact-echo testing is an effective technique to map delaminations on concrete bridge decks and traditionally involves striking the surface with a metal ball or hammer to produce an acoustic response. Traditional excitation techniques have limited deck scanning speeds because of the necessary retrieval of the impactor. In contrast, disposable impactors have the potential advantage of achieving greater deck scanning speeds because they do not need to be retrieved, and they can be combined with air-coupled impact-echo techniques.

For disposable impactors, variability will naturally occur among individual impactors due to even minor differences in impactor composition, geometry, and impact velocity. Such variability means that the resulting acoustic excitation will be inherently stochastic and may therefore offer advantages over the use of a single, uniform impactor. This thesis demonstrates the use of disposable impactors for the detection of shallow delaminations in concrete. Water droplets and ice balls were able to excite the low-frequency flexural modes associated with shallow delaminations in concrete.

6.1 Contributions and Summary

1. Water droplets are environmentally safe, inexpensive, and easily deployed for acoustic excitation. A pressure wave can be produced in the concrete by the water droplet impact because of the "water hammer effect." Two different flow rates were studied in the experiment. Different flows were observed to produce different sized droplets with varying impact parameters. The data presented in Chapter 3 clearly show that the droplets were able to excite the acoustic modes in the concrete associated with shallow delaminations. The use of water in freezing weather conditions may be problematic. Also, the impact force of low-velocity droplets is orders of magnitude below that of

a solid-solid impact [62], which limits the practicality of low-velocity droplets in the field.

2. Ice balls made by freezing potable water are both environmentally friendly and disposable. Ice would melt away quickly if applied during warm seasons and would therefore pose minimal adverse effects on the safety of the traveling public. The spectrograms presented in Chapter 3 of the ice ball impacts on a delaminated concrete surface clearly indicate that the ice balls are capable of exciting the low-frequency flexural modes that are associated with shallow delaminations in the concrete. High-speed photography of representative low-velocity impacts and parametric analysis were used. Calculation results showed that the residence times for the ice spheres were approximately 15 to 85 percent greater than those of the steel ball. The results also indicated that the average force generated by the ice balls was approximately 65 to 80 percent less than that of the steel balls.

3. Results obtained on representative intact and delaminated locations were observed to be consistent for the different sizes of the impactors used in the experiment. However, unlike steel balls and chain links, no clear peaks were observed by ice balls at low flexural frequencies for all of the delaminated locations. Even though the frequency map obtained using ice ball was not very consistent with those obtained from steel ball and chain link, ice ball was able to detect shallow delaminations, and the results agreed with the preliminary chain-drag survey.

6.2 Future Work

The research work done in this thesis can be extended in a few ways.

1. Use of water droplets and ice balls as disposable impactors for acoustic excitation in concrete is presented in this thesis. Future research could include identifying other disposable impactors for the detection of delaminations in concrete. Hertzian theory and high-speed photography could then be applied to estimate the impact characteristics.

2. This thesis proposed the use of water droplets as disposable impactors for delamination detection in concrete. Studying the formation of optimized droplets, focusing particularly on surface tension, density, and viscosity properties, could aid in improving the technique. Additionally, signal processing techniques aimed at reducing the field noise and classifying impacts could be employed. Further tests on controlled concrete substrates and numerical modeling of the impacts will be needed to accurately establish the usable frequency range and penetration depth of this technique. Further, the details of acoustic impact responses by droplets arriving at non–perpendicular angles and/or affected by wind together with surface roughness and hydrophobicity are areas of research that could be explored. It may be that droplets could be used for other materials systems such as composite materials used in aircrafts.

3. Ice balls of three different sizes and their acoustic responses were explored in this thesis. A larger variety of ice ball sizes could be tested to find the optimized size of ice balls required to excite particular frequencies in concrete. Also, the impact velocity and drop height could be optimized. Depth estimation and usable frequency range estimation could be established for the controlled concrete sample. The dispensing system for ice balls could be developed to further deploy the technique in the field. Signal processing tools will have to be implemented to reduce noise and automate classification of defects.

Bibliography

[1] W. Perry, "Grand challenges for engineering." *Technical Report, National Academy of Engineering*, 2008. 1

[2] M. Moore, B. Phares, B. Graybeal, D. Rolander, and G. Washer, "Reliability of visual inspection for highway bridges volume i: Final report. technical report fhwa-rd-01-020," *US Department of Transportation Federal Highway Administration*, 2001. 1

[3] D. Huston, N. Gucunski, A. Maher, J. Cui, D. Burns, and F. Jalinoos, "Bridge deck condition assesment with electromagnetic, acoustic and automated methods," *Sixth international workshop on structural health monitoring, Stanford, CA, USA*, 2007. 1

[4] ASCE, *2013 Report Card for America's Infrastructure*, (2013, 6/17/2013). [Online]. Available: http://www.infrastructurereportcard.org/ 1

[5] "Risk-based transportation asset managment: Managing risks to networks, corridors, and critical structures," *FWHA-HIF-13-017 ed. Washington, DC: Fedral Highway Administration*, 2013. 1

[6] "Bridge preservation guide: Maintaining a state of good repair using cost effective investment strategies," *FWHA-HIF-11-042 ed. Washington, DC: Federal Highway Administration*, 2011. 1

[7] P. D. Carter, "Preventive maintenance of concrete bridge decks," *Concrete International*, vol. 11, pp. 33–36, November 1989. 1

[8] S. Balakumaran, R. E. Weyers, and M. C. Brown, "Modeling corrosion effects," *Concrete*, vol. 35, pp. 47–53, 2013. 2

[9] D. Chen and S. Mahadevan, "Chloride-induced reinforcement corrosion and concrete cracking simulation," *Cement and Concrete Composites*, vol. 30, no. 3, pp. 227 – 238, 2008. 2

[10] C. Li, J. Zheng, W. Lawanwisut, and R. Melchers, "Concrete delamination caused by steel reinforcement corrosion," *Journal of Materials in Civil Engineering*, vol. 19, no. 7, pp. 591–600, 2007. 2

[11] S. Ahmad, "Reinforcement corrosion in concrete structures, its monitoring and service life prediction- review," *Cement and Concrete Composites*, vol. 25, no. 45, pp. 459 – 471, 2003. 2

[12] W. S. Guthrie, C. D. Nolan, and D. P. Bentz, "Effect of initial timing of scarification and overlay treatment on chloride concentrations in concrete bridge decks," *Transportation Research Record*, vol. 2220, pp. 66–74, 2011. 2

[13] N. Gucunski, "Nondestructive testing to identify concrete bridge deck deterioration." *National Research Council (U.S.). Transportation Research Board., and Second Strategic Highway Research Program (U.S.), Washington, DC.: Transportation Research Board*, 2013. 3, 4, 7, 26

[14] N. Gucunski, F. Romero, S. Kruschwitz, R. Feldmann, A. Abu-Hawash, and M. Dunn, "Multiple complementary nondestructive evaluation technologies for condition assessment of concrete bridge decks," *Trasportation Research Board*, vol. 2201, pp. 34–44, 2010. 3

[15] *ASTM Standard D4580 "Standard Practice for measuring Delaminations in Concrete Bridge Decks by Sounding"*, ed. West Conshohocken, PA: ASTM International Std., 2012. 3, 7, 43

[16] M. Sansalone, "Impact-echo: The complete story," *ACI Structural Journal, vol.94, pp. 777-786, Nov-Dec*, 1997. 4, 7, 11, 12, 13

[17] N. Carino, "Training: Often the missing link in using ndt methods," *Construction and Building Materials*, vol. 38, pp. 1316 – 1329, 2013. 4, 7, 12, 20

[18] Y. Tinkey, L. D. Olson, P. Miller, and M. Hergert, "Advances in stress wave scanning of ddeck and pavements," *Engineering mechanics institue conference (EMI 2011), Boston, MA, USA*, 2011. 4

[19] J. Zhu and J. Popovics, "Imaging concrete structures using air-coupled impact-echo," *Journal of Engineering Mechanics*, vol. 133, no. 6, pp. 628–640, 2007. 4, 7, 60

[20] H. Bjurstorm and N. Ryden, "Air-coupled detection of the s1-zgv lamb mode in a concrete plate based on backward wave propagation," *AIP Conference Proceedings*, vol. 1511, pp. 1294–1300, 2013. 4

[21] S. W. Shin, J. S. Popovics, and T. Oh, "Cost effective air-coupled impact-echo sensing for rapid detection of delamination damage in concrete structures." *Advances in Structural Engineering*, vol. 15, no. 6, pp. 887 – 896, 2012. 4

[22] S. Kee, T. Oh, J. Popovics, R. Arndt, and J. Zhu, "Nondestructive bridge deck testing with air-coupled impact-echo and infrared thermography," *Journal of Bridge Engineering*, vol. 17, no. 6, pp. 928–939, 2012. 4, 8

[23] D. Algernon, H. Ernst, and K. Dressler, "Signal processing for air-coupled impact-echo using microphone arrays," *presented at the 18th World Conference on Nondestructive Testing, Durban, South Africa*, 2012. 4

[24] Y. T. Tsai and J. Zhu, "Simulation and experiments of airborne zero-group-velocity lamb waves in concrete plate," *Journal of Nondestructive Evaluation*, vol. 31, no. 4, pp. 373–382, 2012. 4, 11, 13

[25] J. Zhu, "Non-contact ndt of concrete structures using air-coupled sensors," Ph.D. dissertation, PhD, Civil and Environmental Engineering, University of Illinoise at Urbana-Champaign, Urbana, IL, 2005. 4

[26] J. Zhu, J. S. Popovics, and F. Schubert, "Leaky rayleigh and scholte waves at the fluid–solid interface subjected to transient point loading," *The Journal of the Acoustical Society of America*, vol. 116, no. 4, pp. 2101–2110, 2004. 4

[27] X. Dai, J. Zhu, Y. T. Tsai, and M. R. Haberman, "Use of parabolic reflector to amplify in-air signals generated during impact-echo testing," *The Journal of the Acoustical Society of America*, vol. 130, no. 4, pp. EL167–EL172, Oct 2011. 4, 7

[28] X. Dai, M. R. Haberman, Y. T. Tsai, and J. Zhu, "Excitation of rayleigh and zero-group-velocity (zgv) lamb waves using air-borne n-waves focused by an ellipsoidal reflector," vol. 19, no. 1. ASA, 2013, p. 030083. 4

[29] N. Ryden, M. Lowe, and P. Cawley, "Non-contact surface wave scanning of pavements using a rolling microphone array," in *Review of Progress in Quantitative Nondestructive Evaluation*, ser. American Institute of Physics Conference Series, D. O. Thompson and D. E. Chimenti, Eds., vol. 975, Feb. 2009, pp. 1328–1332. 4

[30] G. Zhang, R. Harichandran, and P. Ramuhalli, "Application of noise cancelling and damage detection algorithms in nde of concrete bridge decks using impact signals," *Journal of Nondestructive Evaluation*, vol. 30, no. 4, pp. 259–272, 2011. 4, 23

[31] W. Goldsmith, *Impact: The Theory and Physical Behaviour of Colliding Solids*. London: E. Arnold, 1960. 8

[32] W. J. Stronge, *Impact Mechanics*. Cambridge, England; New York: Cambridge University Press, 2000. 8, 9, 10, 11

[33] M. Ohtsu, M. Yamada, and T. Sonoda, "Quantitative evaluation of sibie procedure and case studies," *Construction and Building Materials*, no. 0, pp. –, 2013. 8

[34] G. C. McLaskey and S. D. Glaser, "Hertzian impact: Experimental study of the force pulse and resulting stress waves," *The Journal of the Acoustical Society of America*, vol. 128, no. 3, pp. 1087–1096, 2010. 10, 11

[35] K. Song and G. C. Cho, "Numerical study on the evaluation of tunnel shotcrete using the impact-echo method coupled with fourier transform and short-time fourier transform," *International Journal of Rock Mechanics and Mining Sciences*, vol. 47, no. 8, pp. 1274 – 1288, 2010. 10

[36] T. K. Oh, "Defect characterization in concrete elements using vibration analysis and imaging," Ph.D. dissertation, PhD, Civil and Environmental Engineering, University of Illinoise at Urbana-Champaign, Urbana, IL, 2012. 11, 13, 14

[37] Y. Zhang and Z. Xie, "Ensemble empirical mode decomposition of impact-echo data for testing concrete structures," *NDT & E International*, vol. 51, no. 0, pp. 74 – 84, 2012. 11

[38] P. L. Liu and P. L. Yeh, "Spectral tomography of concrete structures based on impact echo depth spectra," *NDT & E International*, vol. 44, no. 8, pp. 692 – 702, 2011. 11

[39] A. C. Fischer-Cripps, *Introduction to Contact Mechanics*. 2nd ed. New York: Springer, 2007. 11

[40] F. Schubert and B. Kohler, "Ten lectures on impact-echo," *Journal of Nondestructive Evaluation*, vol. 27, no. 1-3, pp. 5–21, 2008. 11, 13

[41] J. Krautkramer and H. Krautkramer, *Ultrasonic Testing of Materials*. 4th ed. New York: Springer-Verlag, 1990. 11

[42] C. Chang and M. Sansalone, "Effects on impact-echo signals caused by steel reinforcing bars and voids around bars." *ACI MAterials Journal*, vol. 90(5):421-34, 1993. 12

[43] S. D. Holland and D. E. Chimenti, "Air-coupled acoustic imaging with zero-group-velocity lamb modes," *Applied Physics Letters*, vol. 83, no. 13, pp. 2704–2706, 2003. 12

[44] A. Gibson and J. Popovics, "Lamb wave basis for impact-echo method analysis," *Journal of Engineering Mechanics*, vol. 131, no. 4, pp. 438–443, 2005. 12

[45] *ASTM C1383 "Test method for measuring the P-wave speed and the thickness of concrete plates using the impact-echo method.*, Annual book of ASTM standards, vol. 04.02. West Conshohocken (PA): ASTM Std. 13

[46] J. Zhu and J. S. Popovics, "Air-coupled impact-echo method for ndt of concrete," *AIP Conference Proceedings*, vol. 820, no. 1, pp. 1351–1357, 2006. 13

[47] A. G. Piersol and T. L. Paez, *Harri's Shock and Vibration Handbook, 6th ed.* New York: McGraw-Hill, 2010. 14

[48] A. Yarin, "Drop impact dynamics: Splashing, spreading, receding, bouncing," *Annual Review of Fluid Mechanics*, vol. 38, no. 1, pp. 159–192, 2006. 15

[49] M. Sansalone and J. Carino, N, "Detecting delamination in concrete slabs with or without overlays using the impact-echo method," *ACI Materials Journal,*, vol. 86(2), pp. 175–184, 1989. 15

[50] S. Tajiri, M. Tsutahara, and H. Tanaka, "Direct simulation of sound and underwater sound generated by a water drop hitting a water surface using the finite difference lattice boltzmann method," *Computers & Mathematics with Applications*, vol. 59, no. 7, pp. 2411 – 2420, 2010. 15

[51] F. J. Heymann, "High-speed impact between a liquid drop and a solid surface," *Journal of Applied Physics*, vol. 40, no. 13, pp. 5113–5122, 1969. 15, 16, 19

[52] M. B. Lesser, "Analytic solutions of liquid-drop impact problems," *Proceedings of the Royal Society of London. A. Mathematical and Physical Sciences*, vol. 377, no. 1770, pp. 289–308, 1981. [Online]. Available: http://rspa.royalsocietypublishing.org/content/377/1770/289.abstract 15

[53] R. Li, H. Ninokata, and M. Mori, "A numerical study of impact force caused by liquid droplet impingement onto a rigid wall," *Progress in Nuclear Energy*, vol. 53, no. 7, pp. 881 – 885, 2011. 15

[54] D. T. Blackstock, *Fundamentals of Physical Acoustics*. Wiley-Interscience, 2000. 15

[55] M. Mani, S. Mandre, and M. P. Brenner, "Events before droplet splashing on a solid surface," *Journal of Fluid Mechanics*, vol. 647, pp. 163–185, 3 2010. 15

[56] H. H. Shi, K. Takayama, and N. Nagayasu, "The measurement of impact pressure and solid surface response in liquid-solid impact up to hypersonic range," *Wear*, vol. 186(2), no. 0, pp. 352 – 359, 1995. 15

[57] T. Obara, N. Bourne, and J. Field, "Liquid-jet impact on liquid and solid surfaces," *Wear*, vol. 186187, Part 2, no. 0, pp. 388 – 394, 1995, ¡ce:title¿8th International Conference on Erosion by Liquid and Solid Impact¡/ce:title¿. 15

[58] J. Eggers and E. Villermaux, "Physics of liquid jets," *Rep. Prog. Phys.*, vol. 71(3):036601, 2008. 16

[59] X. Zhang and O. A. Basaran, "An experimental study of dynamics of drop formation," *Physics of Fluids*, vol. 7, no. 6, pp. 1184–1203, 1995. 16

[60] H. Chenn, H and P. Brenner, M, "The optimal faucet," *Phys. Rev. Lett.*, vol. 92(16):166106, 2004. 16

[61] C. C. Cheng, Y. Lin, C. M. Hsiao, and H. C. Chang, "Evaluation of simulated transfer functions of concrete plate derived by impact-echo method," *NDT & E International*, vol. 40, no. 3, pp. 239 – 249, 2007. 16

[62] A. S. Grinspan and R. Gnanamoorthy, "Impact force of low velocity liquid droplets measured using piezoelectric {PVDF} film," *Colloids and Surfaces A: Physicochemical and Engineering Aspects*, vol. 356, no. 13, pp. 162 – 168, 2010. 23, 64

[63] F. Schubert, "Impact-echo signature analysis (iesa) a new evaluation procedure for impactecho data based on spectrograms," *European conference on NDT, Berlin, Germany*, p. Fr. 1.4.1, 2006. 23

[64] E. Schulson, "The structure and mechanical behavior of ice," *JOM*, vol. 51, no. 2, pp. 21–27, 1999. 25

[65] M. Montagnat, O. Castelnau, P. Bons, S. Faria, O. Gagliardini, F. Gillet-Chaulet, F. Grennerat, A. Griera, R. Lebensohn, H. Moulinec, J. Roessiger, and P. Suquet, "Multiscale modeling of ice deformation behavior," *Journal of Structural Geology*, no. 0, pp. –, 2013. 25

[66] D. M. Cole, "The microstructure of ice and its influence on mechanical properties," *Engineering Fracture Mechanics*, vol. 68, no. 1718, pp. 1797 – 1822, 2001. 25

[67] P. H. Gammon, H. Kiefte, M. J. Clouter, and W. W. Denner, "Elastic constants of artificial and natural ice samples by brillouin spectroscopy," *Journal of Glaciology*, vol. 29, no. 103, pp. 433–460, 1983. 25

[68] P. Guegan, R. Othman, D. Lebreton, F. Pasco, P. Villedieu, J. Meyssonnier, and S. Witenberger, "Critical impact velocity for ice fragmentation," *Proceedings of the Institution of Mechanical Engineers, Part C: Journal of Mechanical Engineering Science*, 2011. 25, 52

[69] M. Higa, M. Arakawa, and N. Maeno, "Size dependence of restitution coefficients of ice in relation to collision strength," *Icarus*, vol. 133, no. 2, pp. 310 – 320, 1998. 25, 52

[70] B. Federer and A. Waldvogel, "Hail and raindrop size distributions from a swiss multicell storm," *Journal of Applied Meteorology*, vol. 14, pp. 91–97, 1975. 25

[71] N. C. Knight, "Measurement and interpretation of hailstone density and terminal velocity." *Journal of Atmospheric Sciences*, vol. 40, pp. 1510–1516, June 1983. 25

[72] D. L. Mitchell, "Use of mass- and area-dimensional power laws for determining precipitation particle terminal velocities." *Journal of Atmospheric Sciences*, vol. 53, pp. 1710–1723, June 1996. 25

[73] B. J. Frugis and T. A. Wasula, "Development of warning thresholds for one inch or greater hail in the albany new york county warning area," *US Department US Commerce, National Oceanic and Atmospheric Administartion, NAtional Weather Service, Eastern Region*, 2011. 25

[74] T. Marshall, R. Herzog, S. Morrison, and S. Smith, "Hail damage threshold sizes for common roofing materials," *21st Conference on Severe Local Storms, San Antonio, TX*, 2002. 25

[75] I. McNaughton and S. Chisman, "A study of hail impact at high speed on light alloy plates," *DTIC Document 1940*. 26

[76] M. Anghileri, M. L. Castelletti, F. Invernizzi, and M. Mascheroni, "A survey of numerical models for hail impact analysis using explicit finite element codes," *International Journal of Impact Engineering*, vol. 31, no. 8, pp. 929 – 944, 2005. 26

[77] J. D. Tippmann, H. Kim, and J. D. Rhymer, "Experimentally validated strain rate dependent material model for spherical ice impact simulation," *International Journal of Impact Engineering*, vol. 57, no. 0, pp. 43 – 54, 2013. 26

[78] H. Park and H. Kim, "Damage resistance of single lap adhesive composite joints by transverse ice impact," *International Journal of Impact Engineering*, vol. 37, no. 2, pp. 177 – 184, 2010. 26

[79] *ASTM Standard C94 "Standard Specification for Ready-Mixed Concrete"*, ed. West Conshohocken, PA: ASTM International Std., 2013. 26

[80] D. G. Daniel and C. L. Lobo, "User's guide to astm specification c94 on ready-mixed concrete." *West Conshohocken, PA; Silver Spring, MD: ASTM International; NRMCA, National Ready Mixed Concrete Association*, 2005. 26

[81] C. Colla and R. Lausch1, "Influence of source frequency on impact-echo data quality for testing concrete structures," *NDT & E International*, vol. 36, no. 4, pp. 203 – 213, 2003. 36

[82] K. Song and G. C. Cho, "Bonding state evaluation of tunnel shotcrete applied onto hard rocks using the impact-echo method," *NDT & E International*, vol. 42, no. 6, pp. 487 – 500, 2009. 38

[83] S. K. Lin, Y. Lin, K. T. Hsu, and T. Yen, "Use of the normalized impact-echo spectrum to monitor the setting process of mortar," *NDT & E International*, vol. 43, no. 5, pp. 385 – 393, 2010. 39

[84] D. Aggelis, T. Shiotani, and K. Kasai, "Evaluation of grouting in tunnel lining using impact-echo," *Tunnelling and Underground Space Technology*, vol. 23, no. 6, pp. 629 – 637, 2008. 39

[85] G. Zhang, R. S. Harichandran, and P. Ramuhalli, "An automatic impact-based delamination detection system for concrete bridge decks," *NDT & E International*, vol. 45, no. 1, pp. 120 – 127, 2012. 40, 41

[86] M. J. Sansalone and W. B. Streett, *Impact-echo - Nondestructive Evaluation for Concrete and Masonary*. Bullbirer, Ithaca, N.Y., 1997. 46